Report

Neuron

Postingestive Modulation of Food Seeking Depends on Vagus-Mediated Dopamine Neuron Activity

Highlights

- Postingestive sucrose can sustain operant food-seeking behavior
- Intragastric injection of sucrose activates a subpopulation of VTA dopamine neurons
- VTA dopamine neuron bursting is necessary for postingestive-dependent food seeking
- Postingestive modulation of dopamine neuron activity and food seeking is vagus-mediated

Authors

Ana B. Fernandes, Joaquim Alves da Silva, Joana Almeida, Guohong Cui, Charles R. Gerfen, Rui M. Costa, Albino J. Oliveira-Maia

Correspondence

rc3031@columbia.edu (R.M.C.), albino.maia@neuro.fchampalimaud.org (A.J.O.-M.)

In Brief

Fernandes et al. report causal connections between postingestive sucrose sensing and brain dopamine neuron activity in the ventral tegmental area that support food seeking. The authors further demonstrate that such behaviors and the associated neuron activity are mediated by the hepatic branch of the vagus nerve.

Fernandes et al., 2020, Neuron *106*, 1–11
June 3, 2020
https://doi.org/10.1016/j.neuron.2020.03.009

CellPress

Please cite this article in press as: Fernandes et al., Postingestive Modulation of Food Seeking Depends on Vagus-Mediated Dopamine Neuron Activity, Neuron (2020), https://doi.org/10.1016/j.neuron.2020.03.009

Neuron
Report

Postingestive Modulation of Food Seeking Depends on Vagus-Mediated Dopamine Neuron Activity

Ana B. Fernandes,[1,2,3] Joaquim Alves da Silva,[1,2,3] Joana Almeida,[1] Guohong Cui,[4] Charles R. Gerfen,[5] Rui M. Costa,[1,3,6,7,*] and Albino J. Oliveira-Maia[1,2,3,*]
[1]Champalimaud Research, Champalimaud Centre for the Unknown, Lisbon 1400-038, Portugal
[2]Champalimaud Clinical Centre, Champalimaud Centre for the Unknown, Lisbon 1400-038, Portugal
[3]NOVA Medical School | Faculdade de Ciencias Medicas, Universidade Nova de Lisboa, Lisbon 1169-056, Portugal
[4]Neurobiology Laboratory, National Institute of Environmental Health Sciences, NIH, Durham, NC 27709, USA
[5]Laboratory of Systems Neurosciences, National Institute of Mental Health, Bethesda, MD 20814, USA
[6]Departments of Neuroscience and Neurology, Zuckerman Mind Brain Behavior Institute, Columbia University, New York, NY 10027, USA
[7]Lead Contact
*Correspondence: rc3031@columbia.edu (R.M.C.), albino.maia@neuro.fchampalimaud.org (A.J.O.-M.)
https://doi.org/10.1016/j.neuron.2020.03.009

SUMMARY

Postingestive nutrient sensing can induce food preferences. However, much less is known about the ability of postingestive signals to modulate food-seeking behaviors. Here we report a causal connection between postingestive sucrose sensing and vagus-mediated dopamine neuron activity in the ventral tegmental area (VTA), supporting food seeking. The activity of VTA dopamine neurons increases significantly after administration of intragastric sucrose, and deletion of the NMDA receptor in these neurons, which affects bursting and plasticity, abolishes lever pressing for postingestive sucrose delivery. Furthermore, lesions of the hepatic branch of the vagus nerve significantly impair postingestive-dependent VTA dopamine neuron activity and food seeking, whereas optogenetic stimulation of left vagus nerve neurons significantly increases VTA dopamine neuron activity. These data establish a necessary role of vagus-mediated dopamine neuron activity in postingestive-dependent food seeking, which is independent of taste signaling.

INTRODUCTION

Feeding decisions are influenced not only by palatability and environmental food cues but also by the postingestive effects of food, including the effects on energy homeostasis (de Araujo et al., 2012). In fact, postingestive feedback can stimulate ingestive behaviors through conditioning of flavor preferences (Elizalde and Sclafani, 1990; Sclafani, 2004) and even in the absence of orosensory feedback (de Araujo et al., 2008; Oliveira-Maia et al., 2011). Although it has been shown that postingestive nutrient sensing affects feeding behavior, it is not known to which extent these signals influence food-seeking behavior, which is an important component of survival and could have implications for eating-related disorders like obesity. Furthermore, despite evidence of a gut-brain circuit for nutrient sensing (Han et al., 2018; Kaelberer et al., 2018; Tellez et al., 2016), a direct causal link from the periphery to the activity of brain reward areas has not been established. Here we investigated how postingestive nutrient signals modulate dopamine neuron activity to control food-seeking behavior and how these signals are transmitted to the brain to produce such effects.

RESULTS

Postingestive Effects of Sucrose Modulate Operant Food Seeking

We first examined whether postingestive feedback from sucrose could account for food seeking and, specifically, whether it could modulate instrumental lever pressing for sucrose. Food-deprived C57Bl6/J mice were trained to press a lever to obtain oral access to solutions of sucrose or sucralose (a non-caloric artificial sweetener) at concentrations matched for preference (Beeler et al., 2012; Figure 1A). Although lever pressing for both solutions was initially similar, presses sucrose increased much more than for sucralose (Figure 1B), suggesting that postingestive feedback from sucrose contributes to support lever pressing for food. To test whether postingestive sucrose administration is sufficient to support lever pressing, mice were chronically implanted with a gastric catheter for administration of sucrose or sucralose (Ueno et al., 2012). In untrained food-deprived animals, responses to sucrose and sucralose were minimal and not distinguishable (Figures S1A and S1B), suggesting that lever pressing may not be easily associated with postingestive stimulation in the absence of paired orosensory feedback. However, in animals trained under food and water deprivation to lever press for intragastric injections paired with oral delivery of water, robust lever pressing was observed. Indeed, when delivery of water for oral consumption and water deprivation were discontinued, mice pressed solely for intragastric administration of sucrose and were able to escalate lever pressing as required by the reinforcement schedule (Figures 1C and 1D). In contrast, in mice receiving intragastric sucralose, lever pressing did not change (Figure 1D). Furthermore, in a different group of mice, trained similarly but in a simultaneous

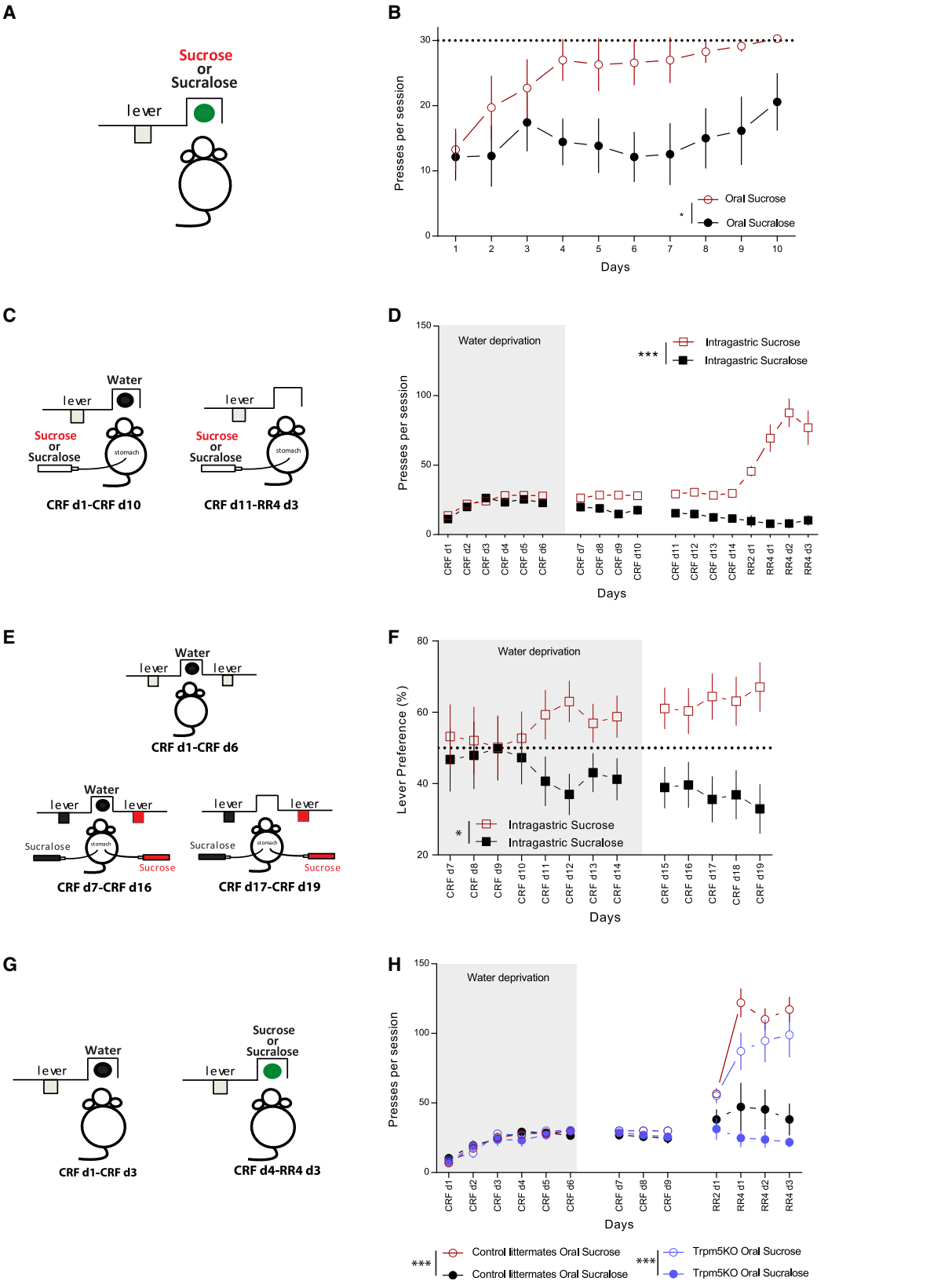

(legend on next page)

2-lever choice task where each lever was associated with intragastric delivery of sucrose or sucralose (Figure 1E), animals developed a preference for the lever associated with intragastric sucrose delivery (Figures 1F, S1C, and S1D), indicating that they are capable of perceiving the contingency between food-seeking actions and their postingestive consequences. Finally, to understand whether these effects could be explained by oral activation of sweet taste receptors via reflux or chemical taste, we tested Trpm5 knockout (KO) mice that are unable to identify sweet taste (Zhang et al., 2003) in a single-lever task as described above but with oral administration of sucralose or sucrose (Figures 1G, S1E, and S1F). Sucrose, but not sucralose, was able to support the escalation of lever pressing (Figure 1H), confirming that these effects depend on postingestive nutrient sensing and not on taste receptor-mediated perception of sweetness.

Intragastric Delivery of Sucrose Activates VTA Dopaminergic Neurons

We next investigated the central mechanisms by which postingestive sucrose could reinforce food-seeking behavior. Feeding-induced dopamine release in the striatum can be driven by postingestive feedback independent of orosensory input (de Araujo et al., 2008; Oliveira-Maia et al., 2011; Tellez et al., 2016). However, a direct effect of postingestive feedback on dopaminergic neuronal activity has not been demonstrated. To explore a potential role of ventral tegmental area (VTA) dopaminergic neurons in postingestive reinforcement of food-seeking behaviors, we monitored VTA dopaminergic neuron activity in freely moving mice during intragastric infusions of sucrose or sucralose performed daily in pseudo-randomized order. VTA dopamine neuron activity was measured in 4 DAT-IRES:Cre (Dopamine Transporter-Internal Ribosome Entry Site-linked Cre recombinase gene) mice using deep-brain calcium imaging (Barretto et al., 2011; Ghosh et al., 2011), as described in STAR Methods (Figures 2A, 2B, and S2A). On average, the activity of 19 neurons was recorded per animal on each day, with no significant differences in the number of neurons between sucrose and sucralose sessions (Figure 2C). Relative to sucralose, the proportion of positively modulated neurons (STAR Methods) after intragastric infusion of sucrose was significantly increased (Figure 2D), whereas activity levels relative to baseline (area under the receiver operating characteristic [ROC] curve [auROC]; STAR Methods) were sustained longer in such sucrose-modulated neurons (Figure S2B). No differences were found for negatively modulated neurons (Figure S2C). Findings were confirmed when restricting analyses to 40 neurons recorded in the last sucrose and the following sucralose sessions (Jennings et al., 2015; Figure 2E), with significantly greater responses to sucrose relative to sucralose (Figure S2D) and more neurons positively modulated by sucrose than sucralose (18 versus 8 of 40 neurons, respectively; $p < 0.02$, McNemar test; Figure 2F). Our findings were equivalent when comparing neurons recorded in the last sucrose and the previous rather than the following sucralose session (Figures S2E and S2F). Importantly, measures of movement did not differ between sucrose and sucralose sessions (Figure 2G), indicating that this did not underlie differences in VTA dopamine neural activity between the two conditions. In a second set of 3 DAT-IRES:Cre mice, we found that the response of VTA dopaminergic neurons to intragastric sucrose infusion did not differ according to food deprivation state (Figures S3A–S3D). In one of these DAT-IRES:Cre mice, tested under food deprivation, we found that VTA dopamine neural activity was increased during licking for sucrose compared with activity during intragastric sucrose and oral sucralose (Figures S3E–S3G), further suggesting that responses to oral and postingestive stimulation are additive. Overall, these data reveal that postingestive effects of sucrose are sufficient to induce sustained activity in VTA dopaminergic neurons.

Bursting of VTA Dopaminergic Neurons Is Necessary for Postingestion-Dependent Food Seeking

To test whether VTA dopaminergic neuron activity is necessary for postingestive food seeking, we generated mice with altered N-Methyl-D-Aspartate (NMDA)-dependent bursting in dopaminergic cells, resulting in reduced phasic responses to reward-predicting stimuli and during learning as well as altered plasticity (Parker et al., 2010; Zweifel et al., 2009). Cell type specificity and

Figure 1. Postingestive Modulation of Food Seeking

(A) Food-deprived mice were trained to press a lever to obtain sucrose or sucralose for oral consumption.

(B) Number of lever presses per session for 7 mice reinforced with sucrose and 7 others reinforced with sucralose (main effect for reinforcer: $F_{1,12} = 5.99$, *$p = 0.04$; two-way ANOVA).

(C) Water- and food-deprived mice lever-pressed to obtain water for oral consumption concomitantly with infusion of a reinforcer through an intragastric catheter. After several days of continuous reinforcement (CRF) sessions, delivery of water during the task and water deprivation in the home cage were discontinued, with lever pressing resulting solely in administration of intragastric solutions. During the last days (right panel), mice started a random ratio schedule (RR2 or RR4, i.e., reinforcer delivery, on average, every 2 or 4 lever presses, respectively).

(D) Number of lever presses per session for mice receiving intragastric sucrose (n = 12) or intragastric sucralose (n = 10; main effect for reinforcer: $F_{1,20} = 87.1$, ***$p < 0.0001$; two-way ANOVA).

(E) Water- and food-deprived mice with 2 intragastric catheters were trained to press either of two levers to obtain oral water (top panel). After 6 days, in addition to oral water, intragastric sucrose was assigned to one lever and intragastric sucralose to the other lever (bottom left panel). During the last days of training, lever pressing resulted solely in intragastric infusion (bottom right panel).

(F) Lever preference associated with intragastric sucrose or sucralose administration (n = 13; main effect for reinforcer: $F_{1,12} = 6.68$, *$p = 0.02$; two-way repeated-measures ANOVA).

(G) Food- and water-deprived Trpm5 KO mice trained in CRF sessions to lever-press initially for oral water (left panel) and later for sucrose or sucralose for oral consumption (right panel), with transition to RR and discontinuation of water deprivation as described in (C).

(H) Number of lever presses per session for sucrose (n = 7) or sucralose (n = 8) in Trpm5 KO mice (main effect for reinforcer: $F_{1,12} = 18.2$, ***$p = 0.001$; two-way ANOVA) and control littermate mice (sucrose, n = 9; sucralose, n = 8; main effect for reinforcer: $F_{1,15} = 15.4$, ***$p = 0.001$; two-way ANOVA).

Data are presented as mean ± SEM. Grey bars indicates the period of water deprivation. For detailed statistical analysis, see Table S1.

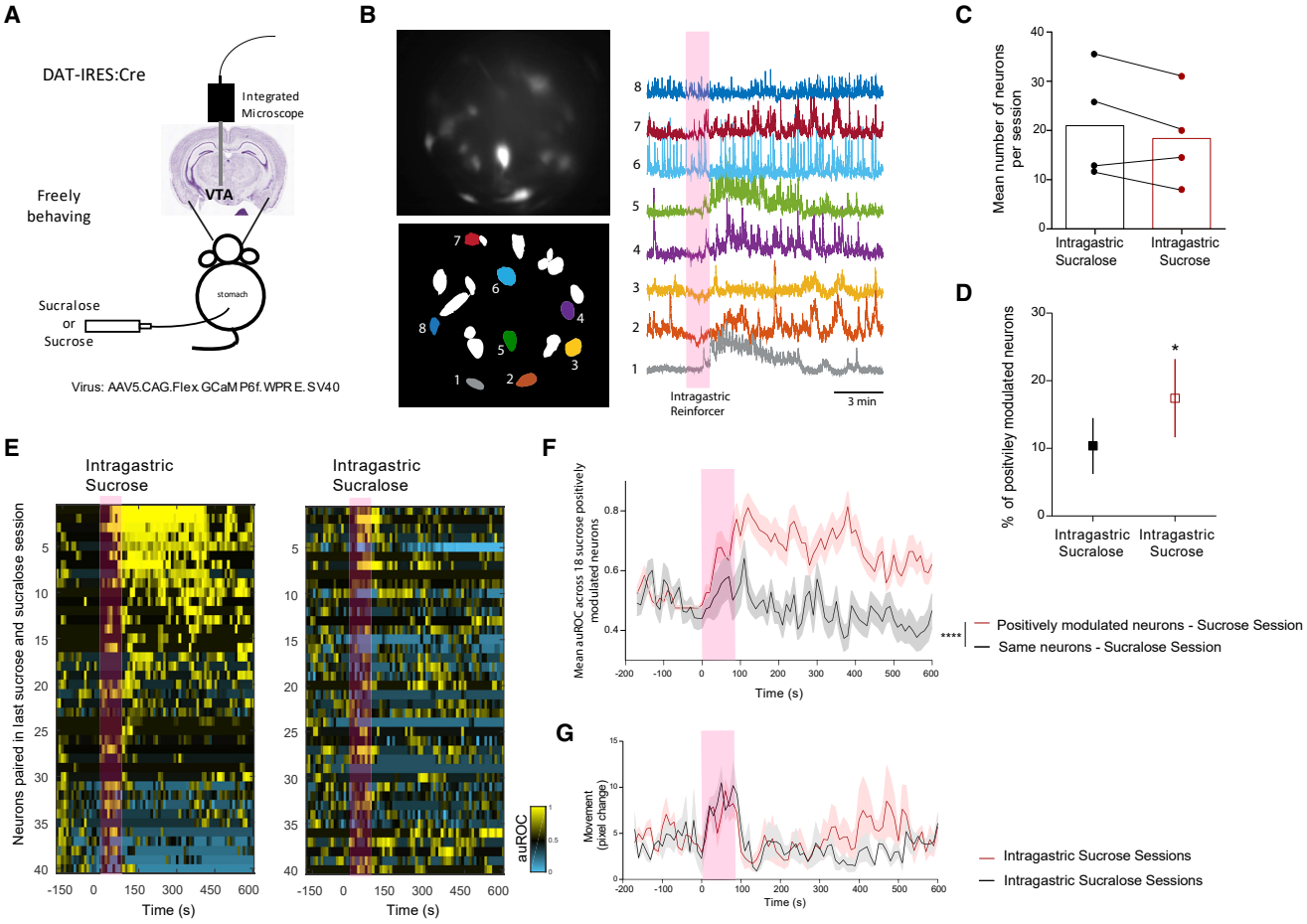

Figure 2. VTA Dopaminergic Neuron Activity in Freely Behaving Mice during Intragastric Delivery of Reinforcers

(A) In 4 DAT-IRES:Cre mice, a miniature microscope was used for deep-brain calcium imaging from VTA dopaminergic neurons during intragastric sucrose or sucralose administration.

(B) Examples of VTA dopaminergic neurons during a sucrose session (top left panel) and the respective regions of interest (bottom left panel), with a time course of the fluorescence traces for some of these neurons, coded according to numbers and colors, are shown in the right panel. In this and other panels, a pink bar represents reinforcer delivery.

(C) Average number of neurons recorded in intragastric sucralose and sucrose sessions per mouse ($p = 0.2$, paired t test).

(D) Percentage of positively modulated neurons per mouse, comparing intragastric sucrose and sucralose delivery (*$p = 0.03$, paired t test). Data are presented as mean ± SEM.

(E) Activity of 40 neurons recorded in the last sucrose (left panel) and the following sucralose session (right panel). Each line in represents a single neuron, with a color code for change in neuronal activity relative to baseline, defined according to the auROC (STAR Methods) in consecutive 10-s bins.

(F) Mean activity of 18 neurons represented in (E) that were positively modulated by intragastric sucrose, comparing responses in the last sucrose and following sucralose sessions ($F_{1,17} = 34.3$, ****$p < 0.0001$; two-way repeated-measures ANOVA; shading indicates SEM).

(G) Mean animal movement during sucrose and sucralose sessions ($F_{1,2} = 0.3$, $p = 0.6$; two-way repeated-measures ANOVA; shading indicates SEM).

For detailed statistical analysis, see Table S1.

distribution patterns were achieved with a *Th*-Cre mouse line, expressing Cre recombinase in tyrosine hydroxylase gene (*Th*) expressing neurons mostly in the VTA (Gong et al., 2007), and were confirmed by breeding with Cre reporter mice expressing green fluorescent protein (GFP) only in Cre-expressing cells (Tanahira et al., 2009). Double immunostaining for tyrosine hydroxylase (TH) and GFP confirmed Cre recombination mostly in dopaminergic neurons in the VTA, partially in the *substantia nigra pars compacta* (SNc), and only residually in the *locus coereleus* (LC; Figures 3A and 3B). *Th*-Cre mice were then crossed with mice carrying a floxed allele of the *Grin1* gene, encoding the NR1 subunit of NMDA receptors (NMDARs), to generate mice with NR1 KO in TH neurons (Jin and Costa, 2010; Ramsey et al., 2011), to which we will refer as Th-CreNR1KO mice. To verify cell-type-specific NMDAR deletion in these mice, we performed whole-cell recording in acute brain slices to measure electrical stimulation-evoked, NMDAR-mediated excitatory postsynaptic currents (I_{NMDA}s). In Th-CreNR1KO mice, I_{NMDA}s were detected in only 1 of 22 recorded VTA dopaminergic cells, whereas in control mice, they were detected in all VTA dopaminergic (5 of 5 recorded) and LC norepinephrine (5 of 5 recorded) neurons (Figures 3C and 3D). Consistent with the results from the

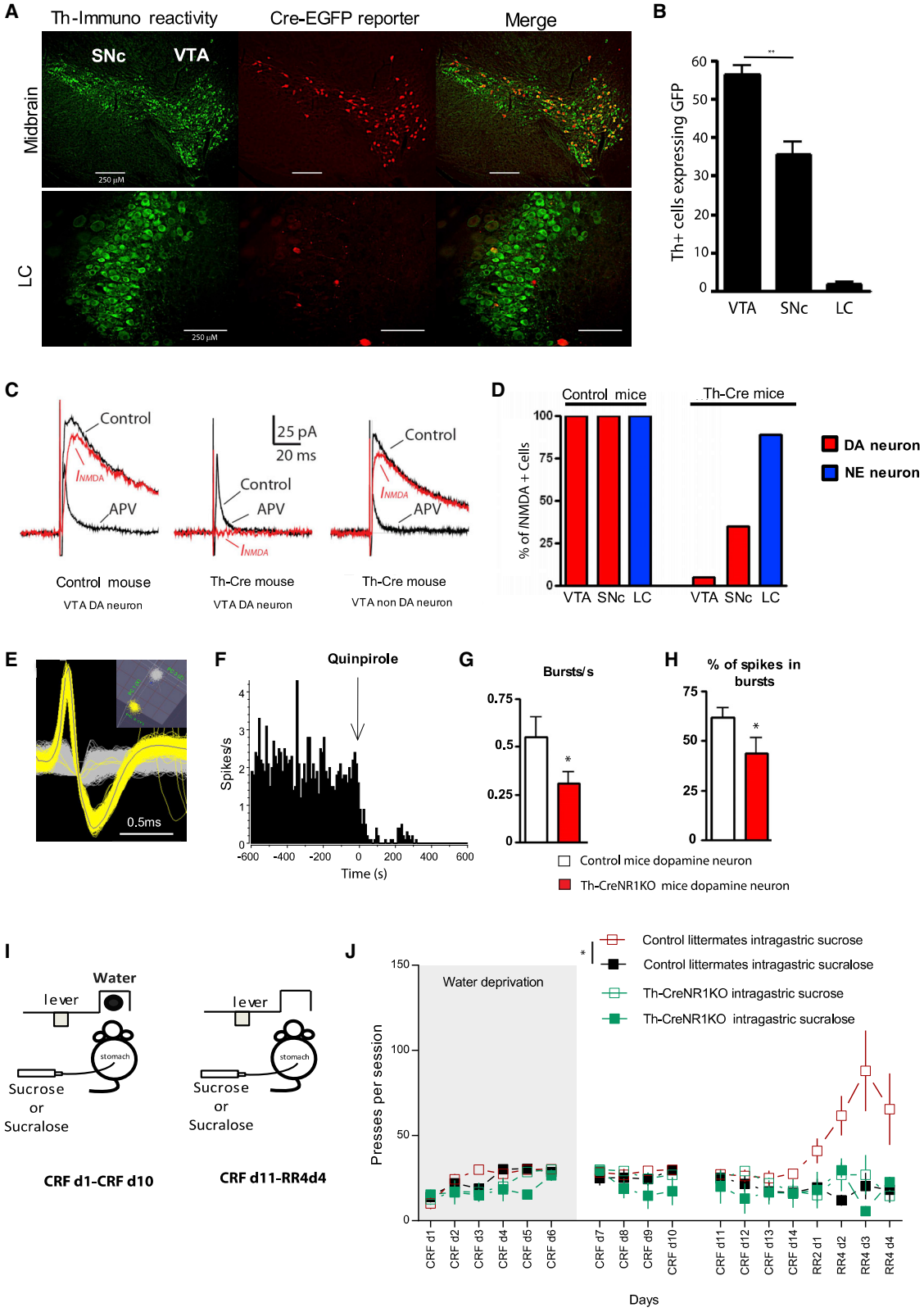

(legend on next page)

GFP reporter mice, in Th-CreNR1KO mice, I_{NMDA}s were detected in 11 of 32 recorded SNc dopaminergic neurons and 8 of 9 recorded LC norepinephrine neurons (Figure 3D), indicating that the LC was mostly spared and that the SNc was affected to a lesser extent than the VTA. To assess burst activity of VTA dopamine neurons in awake and freely moving mice, we implanted multi-electrode microwire arrays in the VTA and recorded the activity of putative dopaminergic neurons, identified according to waveform, basal firing rate, and sensitivity to the dopamine D2 receptor agonist quinpirole (Jin and Costa, 2010; Figures 3E and 3F). At baseline, Th-CreNR1KO mice had lower numbers of burst events and spikes fired in bursts (Figures 3G and 3H) in VTA dopaminergic neurons that also had impaired phasic responses to reward-predicting stimuli (Figure S4). We then tested whether the ability of intragastric sucrose to reinforce food-seeking behavior, as described above, was impaired in Th-CreNR1KO mice (Figure 3I). In control mice, as expected, intragastric sucrose resulted in significantly more lever pressing than intragastric sucralose. Th-CreNR1KO mice, however, did not increase pressing to intragastric sucrose and exhibited similar lever-pressing behavior for intragastric sucrose and sucralose (Figure 3J). These results indicate that NMDA-dependent bursting and/or plasticity in dopaminergic VTA neurons is necessary for postingestive sucrose to reinforce lever-pressing behavior.

Postingestive Modulation of Food Seeking and Dopamine Neuron Activity Depends on the Hepatic Branch of the Vagus Nerve

Despite abundant evidence of a gut-brain axis, the mechanisms by which postingestive nutrient-related signals lead to dopaminergic and behavioral effects are less known. Although there is evidence that vagus nerve lesions disrupt flavor-nutrient conditioning (Zafra et al., 2007), its role in conditioning by nutrients is controversial (Sclafani and Lucas, 1996), and there are also reports of hormonal factors affecting nutrient sensing (Cone et al., 2014; Figlewicz et al., 2003; Klok et al., 2007). Variability in the behavioral effects of vagotomy may result from several methodological differences, such as the nutrient and how it is administered (Qu et al., 2019) or, importantly, the nerve branch that is lesioned (Dixon et al., 2000). Given prior studies suggesting the hepatic vagus nerve (HVN) as a possible candidate for conduction of postingestive nutrient information (Oliveira-Maia et al., 2011; Zafra et al., 2007; Zhang et al., 2018), we tested whether denervation of the HVN impacted the effects of postingestive sucrose on VTA dopaminergic activity and reinforcement of food seeking. VTA dopaminergic activity during intragastric infusion of sucrose or sucralose was measured using deep-brain calcium imaging, as described above, in 3 DAT-IRES:Cre mice surgically denervated at the HVN and 3 others receiving sham surgery. HVN denervation did not affect the mean number of neurons recorded per session in each animal (Figure 4A). As expected, sham-operated mice had a significant increase in VTA dopaminergic activity in intragastric sucrose compared with sucralose sessions (Figure 4B), an effect that was conserved when analyses were restricted to the first or the last sucrose and sucralose sessions (data not shown). In this group, the proportion of positively modulated neurons was also higher in sucrose sessions (Figure 4C). In the vagotomy group, however, VTA dopaminergic activity (Figure 4D) as well as the proportion of positively modulated neurons (Figure 4E) did not differ between sucrose and sucralose sessions. Tracking of single neurons recorded in the last sucralose and the following sucrose session (Figures 4F and 4G) confirmed a significantly greater proportion of neurons positively modulated by sucrose relative to sucralose in the sham (26 versus 15 of 46 neurons, respectively; $p < 0.02$, McNemar test; Figure 4F) but not the vagotomy group (16 versus 19 of 50 neurons, respectively; $p = 0.8$, McNemar test; Figure 4G), resulting in significant differences in sucrose-modulated neurons in the sham relative to the vagotomy group (57% versus 32%; Figure 4H). Importantly, for the vagotomy group, even though visual inspection of single-cell dopaminergic activity plots (Figure 4G) suggests that the effects of sucrose are longer lasting, a direct comparison of the activity of these neurons in the sucrose and sucralose sessions did not reveal a significant effect for reinforcer. However, it revealed a significant time-reinforcer interaction that may reflect a residual HVN-independent effect of intragastric sucrose. Finally, we performed the postingestive behavioral reinforcement protocol described above in a different set of C57Bl6/J mice (Figure 4I) and found that, compared with sham-operated mice, those with HVN lesions had significantly

Figure 3. NMDA-Dependent Bursting in Dopaminergic Neurons Is Necessary for Postingestive-Dependent Food-Seeking Behavior

(A) Example midbrain (ventral tegmental area [VTA] and *substantia nigra pars compacta* [SNc]) and *locus coereleus* (LC) coronal sections of double immunofluorescence staining for tyrosine hydroxylase (TH) and green fluorescent protein (GFP) in double-transgenic Cre reporter mice.

(B) Percentage of TH+ neurons expressing GFP in 6 midbrain sections and 4 LC sections from 2 mice (**$p < 0.01$, paired t test comparing the VTA and SNc).

(C) Representative traces (average of 10 sweeps, with voltage held at +40 mV) of electrically evoked NMDA currents (I_{NMDA}s) in VTA dopamine neurons of control mice as well as dopamine and non-dopamine neurons of Th-CreNR1KO mice. I_{NMDA}s were isolated by subtracting the excitatory postsynaptic current (EPSC) in the presence of APV (2-amino-5-phosphonovaleric acid, an NMDAR antagonist) from the pre-APV EPSC.

(D) Percentage of recorded cells in which I_{NMDA}s were detected among 3 control and 14 Th-CreNR1KO mice.

(E) Example action potential waveforms (yellow traces) of a putative dopamine neuron recorded in a freely moving mouse using microwire metal electrodes. The inset depicts the separation of the recorded single unit (yellow) from noise (gray) in a 3-dimentional principal-component analysis.

(F) Firing rate of the neuron shown in (E) and its response to quinpirole (200 μg/kg intraperitoneally [i.p.]).

(G and H) Bursts per second (G) and percentage of spikes fired in bursts (H) in 26 and 14 dopamine neurons from control mice and Th-CreNR1KO mice, respectively (* $p<0.05$, unpaired t tests).

(I) Th-CreNR1KO mice and control littermates performed a behavioral task as described in Figure 1C.

(J) Number of lever presses per session in Th-CreNR1KO mice pressing for either intragastric sucrose ($n = 5$) or sucralose ($n = 3$; main effect for reinforcer: $F_{1,6} = 1.4$, $p = 0.3$; two-way ANOVA) and control littermate mice (sucrose, $n = 6$; sucralose, $n = 5$; main effect for reinforcer: $F_{1,9} = 7.8$, *$p = 0.02$; two-way ANOVA). Grey bar indicates the period of water deprivation.

Data are presented as mean ± SEM. For detailed statistical analysis, see Table S1.

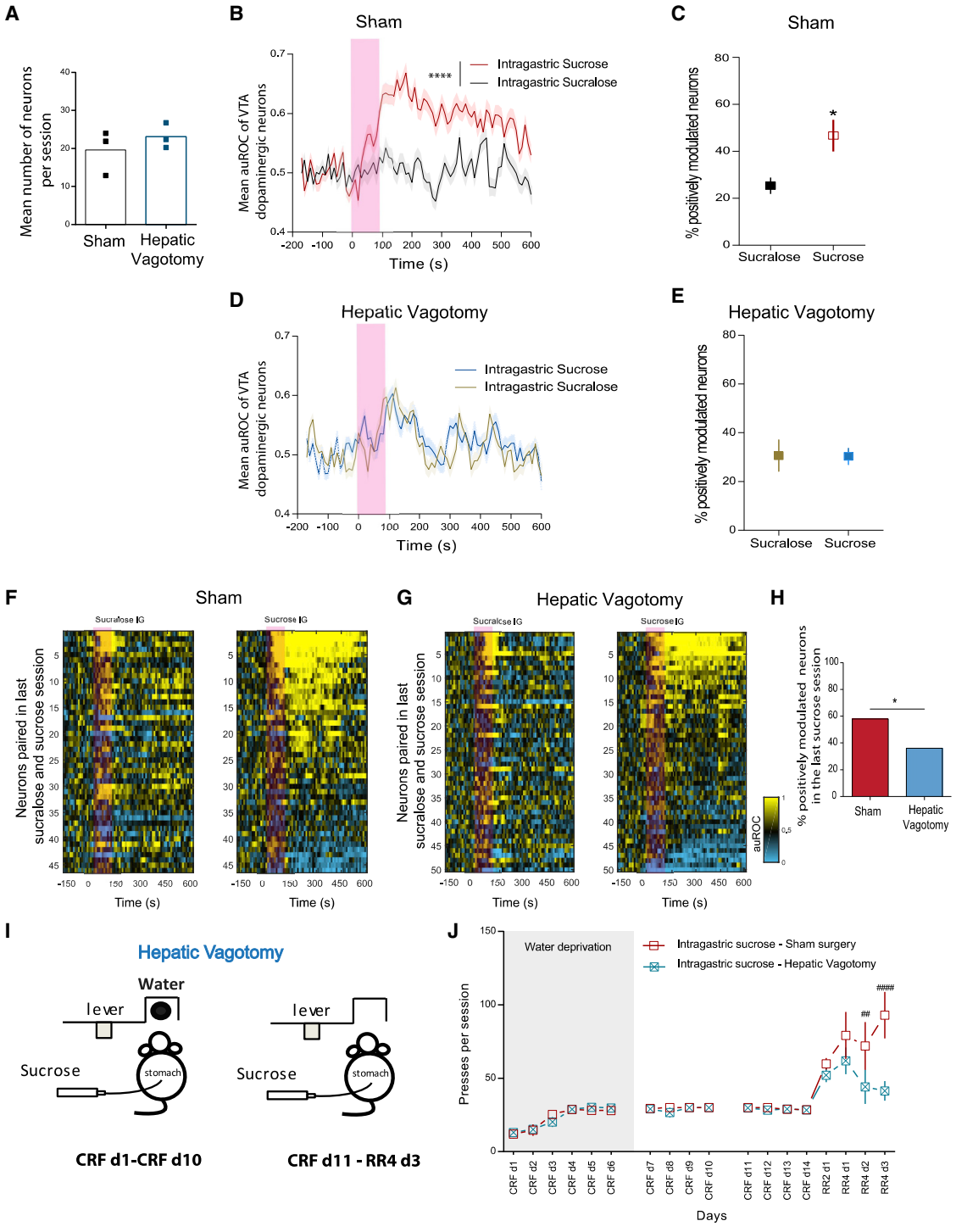

Figure 4. VTA Dopaminergic Neuron Activity in Response to Postingestive Sucrose Is Dependent on the Hepatic Branch of the Vagus Nerve

Calcium imaging of VTA dopamine neurons was performed in 3 DAT-IRES:Cre mice with hepatic vagus nerve (HVN) denervation and 3 mice receiving sham surgery, as described above.

(A) Total number of neurons recorded per session in denervated and sham mice ($p = 0.4$, unpaired t test).

(B–E) Neuronal activity relative to baseline (auROC) in VTA dopaminergic neurons recorded during intragastric sucrose and sucralose sessions in sham (B; sucrose, n = 249 neurons; sucralose, n = 221 neurons; main effect for reinforcer: $F_{1,50544} = 674.7$, ****$p < 0.0001$; two-way ANOVA) and denervated mice (D; sucrose, n = 299; sucralose, n = 263; main effect for reinforcer: $F_{1,60480} = 3.5$, $p = 0.6$; two-way ANOVA; shading indicates SEM). Also shown is the mean

(legend continued on next page)

fewer, but not completely abolished, instrumental responses to postingestive sucrose (Figure 4J). These results confirm that signaling through the hepatic branch of the vagus nerve has a critical role in postingestive modulation of VTA dopaminergic activity and food-seeking behavior.

Importantly, we also explored whether vagus nerve stimulation could, per se, modulate VTA dopamine neuron activity. Initially, we investigated hepatic vagal innervation with retrograde labeling using a retrograde adeno-associated virus (AAVRg-GFP) injected at the hepatic hylus enervation and vasculature and found significantly more GFP-marked axons and cell bodies in the left than the right nodose ganglion (Figure S6A), suggesting asymmetric representation of afferent HVN sensory information. Based on these results, we injected an AAV-ChR2 virus in the left nodose ganglion (LNG) of DAT-IRES:Cre mice (Figure S6B), and placed an LED over the ganglion for light delivery and optogenetic stimulation of LNG neurons during imaging of VTA dopaminergic neuron activity (Figure S6C). LNG stimulation significantly increased the activity of VTA dopaminergic neurons relative to baseline, compared with the effects of the same stimulation protocol in animals injected with an AAV-YFP (Yellow Fluorescent Protein) virus in the LNG and, thus, without ChR2 expression (Figures S6D and S6E).

DISCUSSION

Our results show that postingestive sucrose supports robust food seeking through modulation of dopaminergic VTA neuron activity, which is largely dependent on information transmitted by the hepatic branch of the vagus nerve. While previous evidence suggested that nutrient sensing is important for ingestive behavior using food preference assays (de Araujo et al., 2008; Oliveira-Maia et al., 2011; Sclafani, 2004; Sclafani et al., 2015; Zukerman et al., 2011), here we found that postingestive nutrient sensing is sufficient to support and robustly modulate previously established food seeking behaviors. Furthermore, we demonstrated causal links between postingestive feedback and VTA dopaminergic activity mediating such food-seeking behaviors. Specifically, we identified a population of VTA dopaminergic neurons that dynamically responds to postingestive sucrose, probably underlying prior evidence for striatal dopamine release upon postingestive stimulation (Beeler et al., 2012; de Araujo et al., 2008; Han et al., 2018; Oliveira-Maia et al., 2011; Tellez et al., 2016), and established that NMDA-dependent bursting/plasticity in VTA dopaminergic neurons is necessary for postingestive reinforcement of food-seeking behaviors. Finally, we demonstrated that the hepatic branch of the vagus nerve is largely responsible for the effects of postingestive sucrose on food-seeking behaviors and VTA dopaminergic activity. Moreover, stimulation of neurons in the LNG was found to cause increase of VTA dopaminergic activity, supporting that sensory information from the hepato-portal system is conveyed to the VTA through this ganglion of the vagus nerve.

These results strongly support a role of nutrient-stimulated dopamine neuron activity in the regulation of food seeking (Wise, 2006), with postingestive feedback sustaining, but not initiating, food-seeking actions. Importantly, we found that the activity of VTA dopamine neurons was significantly enhanced when mice licked for oral sucrose compared with intragastric sucrose or oral sucralose, suggesting that oral signals, fundamental to drive initiation of food seeking, are associated with a dopamine signal that is at least partially independent of, and cumulative with, the postingestive dopamine signal. Findings in a 2-lever condition, where postingestive stimulation induced a gradual preference for one of two previously acquired actions, developing across days, suggest that such stimulation and the associated dopamine neuron activity act, at least in part, through learning about consequences of actions. Specifically, postingestive-related dopamine signals, which are necessarily slower and presumably less explicit than those associated with explicit and fast orosensory feedback, may be associated with identification and tracking of differential postingestive effects across days, according to spontaneous variability in sampling from the available options, with development of progressive preferences for actions leading to greater postingestive stimulation.

The mechanism by which postingestive sucrose leads to increased VTA dopaminergic neuron activity via the HVN could be similar to that involving neuropod cells, recently identified in the gut and shown to synapse with the vagus nerve (Kaelberer et al., 2018). Another recent study, showing that stimulation of neurons in the right nodose ganglion, but not the LNG, leads to an SNc-mediated increase in striatal dopamine release (Han et al., 2018), provided limited insight on how this pathway is relevant for nutrient sensing. In contrast, our study uncovered a pathway between the HVN, transmitting postingestive information about carbohydrates via the LNG, and dopamine neuron activity in the VTA. Importantly, hepatic denervation experiments did not completely abolish lever pressing behavior to obtain intragastric sucrose, and it is possible that residual VTA dopaminergic activity in response to intragastric sucrose may have persisted even after HVN lesions, suggesting that other neural pathways and/or other hormonal or humoral mechanisms can

proportion of positively modulated neurons per session, comparing sucrose and sucralose sessions in sham (C; *p = 0.03) and denervated mice (E; p = 0.98, paired t tests). In this and other panels, a pink bar indicates the time of the reinforcer injection.

(F) VTA single neuron activity in sham mice recorded in the last sucralose (left panel) and the following intragastric sucrose (right panel) sessions. Each line represents a single neuron with a color code for variation of neuronal activity relative to baseline (auROC) in consecutive 10-s bins.

(G) Analysis described in (F) for denervated mice.

(H) Percentage of positively modulated neurons in the last sucrose session in the sham and denervated groups (*p = 0.02; Fisher's exact test).

(I) Behavioral task progressing to lever pressing for intragastric sucrose infusion, as described in Figure 1C, in mice randomly assigned to hepatic vagus denervation (n = 9) or sham surgery (n = 8).

(J) Lever pressing for intragastric sucrose comparing sham and denervated mice (main effect for group: $F_{1,15} = 3.8$, p = 0.07; group-day interaction: $F_{17,255} = 3.4$, p < 0.0001; two-way ANOVA; post hoc comparisons between sham and denervated mice on each day, ##p < 0.01, ####p < 0.001). Grey bar indicates the period of water deprivation.

Data are presented as mean ± SEM. For detailed statistical analysis, see Table S1.

contribute to transmit the nutritional value of food to mesolimbic dopamine circuits (Cone et al., 2014; Figlewicz et al., 2003; Floresco et al., 2003; Han et al., 2018; Klok et al., 2007; Naleid et al., 2005; Steinbusch et al., 2015). Nevertheless, we note that, in rats with abdominal vagotomy sparing the HVN, the conditioning effects of an intragastric carbohydrate were conserved (Sclafani and Lucas, 1996).

Naturally, other brain areas and circuits, beyond dopaminergic circuits involving the VTA, are expected to contribute to postingestive-dependent behaviors. The contribution of hypothalamic neurons, given their well-known role in modulating feeding behaviors (Atasoy et al., 2012; Sternson et al., 2013), may be particularly relevant. Two recent studies have demonstrated that Agouti-related protein (AgRP)-positive neurons in the arcuate nucleus respond rapidly and transiently to preingestive stimulation, with a slower and more sustained response to postingestive stimulation, through a mechanism that is energy, rather than nutrient dependent (Beutler et al., 2017; Su et al., 2017). The response of hypothalamic AgRP neurons to intragastric injection of nutrients thus has commonalities with the results reported here for VTA dopaminergic neurons, and it is possible that the two responses may be causally associated (Godfrey and Borgland, 2019). Recently, others have demonstrated that AgRP neurons are inhibited through vagal neurons that are sensitive to intestinal mechanoreceptors (Bai et al., 2019) that can be stimulated even in the absence of nutrients. Thus, distinct gastrointestinal and visceral signals, responding across different timescales to ingestion of different nutrients, may lead to diverse and complex patterns of activation and inhibition across several brain areas, providing information about the characteristics of the food that was ingested (Bai et al., 2019; Beutler et al., 2017; Su et al., 2017).

In conclusion, we demonstrated that postingestive nutrient signals lead to modulation of VTA dopaminergic activity, which is required for postingestive modulation of food seeking. Viscerosensory signals sustaining these phenomena are largely transmitted through the hepatic branch of the vagus nerve, which is necessary for VTA dopaminergic neuron activation and behavioral conditioning in response to postingestive sucrose. Our results provide critical contributions to understanding central and peripheral mechanisms underlying food-seeking behavior, with potential effects on future advances in the treatment and prevention of obesity.

STAR★METHODS

Detailed methods are provided in the online version of this paper and include the following:

SUPPLEMENTAL INFORMATION

Supplemental Information can be found online at https://doi.org/10.1016/j.neuron.2020.03.009.

ACKNOWLEDGMENTS

This work was supported by Fundação para a Ciência e Tecnologia (FCT) through a postdoctoral fellowship (SFRH/BPD/880972/2012 to A.B.F.) and grant 030845, co-funded by FEDER under the Lisboa2020 Partnership Agreement (to A.B.F., R.M.C., J.A.d.S., and A.J.O.-M.); by a doctoral fellowship from the Gulbenkian Foundation (to J.A.d.S.); by the Intramural Research Program of the NIMH (ZIA-MH002497-29 to C.R.G.); by ERA-NET, ERC (COG 617142), and HHMI (IEC 55007415) (to R.M.C.); and by the BIAL Foundation (176/10) and the AXA Research Fund (to A.J.O.-M.). Further support was obtained from the research infrastructure Congento, co-funded by Lisboa2020 and FCT (LISBOA-01-0145-FEDER-022170).

AUTHOR CONTRIBUTIONS

A.B.F., J.A.d.S., R.M.C., and A.J.O.-M. designed experiments and conceptualized and performed analyses. A.B.F., J.A.d.S., and J.A. performed behavioral, calcium imaging, and histology experiment analyses. G.C. and C.R.G. characterized cell-type-specific deletion of neuronal NMDARs. A.B.F. wrote the original draft with J.A.d.S., R.M.C., and A.J.O.-M., and it was critically reviewed by the other authors. R.M.C. and A.J.O.-M. supervised the work.

DECLARATION OF INTERESTS

A.J.O.-M. is the recipient of a grant from Schuhfried GmBH for norming and validation of cognitive tests and the national coordinator for Portugal of a non-interventional Study (EDMS-ERI-143085581, 4.0) sponsored by Janssen-Cilag Ltd., both outside of this work.

Received: November 22, 2018
Revised: February 7, 2020
Accepted: March 12, 2020
Published: April 6, 2020

REFERENCES

Atasoy, D., Betley, J.N., Su, H.H., and Sternson, S.M. (2012). Deconstruction of a neural circuit for hunger. Nature *488*, 172–177.

Bai, L., Mesgarzadeh, S., Ramesh, K.S., Huey, E.L., Liu, Y., Gray, L.A., Aitken, T.J., Chen, Y., Beutler, L.R., Ahn, J.S., et al. (2019). Genetic Identification of Vagal Sensory Neurons That Control Feeding. Cell *179*, 1129–1143.e23.

Barretto, R.P.J., Ko, T.H., Jung, J.C., Wang, T.J., Capps, G., Waters, A.C., Ziv, Y., Attardo, A., Recht, L., and Schnitzer, M.J. (2011). Time-lapse imaging of disease progression in deep brain areas using fluorescence microendoscopy. Nat. Med. *17*, 223–228.

Beeler, J.A., McCutcheon, J.E., Cao, Z.F.H., Murakami, M., Alexander, E., Roitman, M.F., and Zhuang, X. (2012). Taste uncoupled from nutrition fails to sustain the reinforcing properties of food. Eur. J. Neurosci. *36*, 2533–2546.

Beutler, L.R., Chen, Y., Ahn, J.S., Lin, Y.C., Essner, R.A., and Knight, Z.A. (2017). Dynamics of Gut-Brain Communication Underlying Hunger. Neuron *96*, 461–475.e5.

Cohen, J.Y., Haesler, S., Vong, L., Lowell, B.B., and Uchida, N. (2012). Neuron-type-specific signals for reward and punishment in the ventral tegmental area. Nature *482*, 85–88.

Cone, J.J., McCutcheon, J.E., and Roitman, M.F. (2014). Ghrelin acts as an interface between physiological state and phasic dopamine signaling. J. Neurosci. *34*, 4905–4913.

Costa, R.M., Lin, S.-C., Sotnikova, T.D., Cyr, M., Gainetdinov, R.R., Caron, M.G., and Nicolelis, M.A.L. (2006). Rapid alterations in corticostriatal ensemble coordination during acute dopamine-dependent motor dysfunction. Neuron *52*, 359–369.

da Silva, J.A., Tecuapetla, F., Paixão, V., and Costa, R.M. (2018). Dopamine neuron activity before action initiation gates and invigorates future movements. Nature *554*, 244–248.

de Araujo, I.E., Oliveira-Maia, A.J., Sotnikova, T.D., Gainetdinov, R.R., Caron, M.G., Nicolelis, M.A.L., and Simon, S.A. (2008). Food reward in the absence of taste receptor signaling. Neuron *57*, 930–941.

de Araujo, I.E., Ferreira, J.G., Tellez, L.A., Ren, X., and Yeckel, C.W. (2012). The gut-brain dopamine axis: a regulatory system for caloric intake. Physiol. Behav. *106*, 394–399.

Dias-Ferreira, E., Sousa, J.C., Melo, I., Morgado, P., Mesquita, A.R., Cerqueira, J.J., Costa, R.M., and Sousa, N. (2009). Chronic stress causes frontostriatal reorganization and affects decision-making. Science *325*, 621–625.

Dixon, K.D., Williams, F.E., Wiggins, R.L., Pavelka, J., Lucente, J., Bellinger, L.L., and Gietzen, D.W. (2000). Differential effects of selective vagotomy and tropisetron in aminoprivic feeding. Am. J. Physiol. Regul. Integr. Comp. Physiol. *279*, R997–R1009.

Elizalde, G., and Sclafani, A. (1990). Flavor preferences conditioned by intragastric polycose infusions: a detailed analysis using an electronic esophagus preparation. Physiol. Behav. *47*, 63–77.

Figlewicz, D.P., Evans, S.B., Murphy, J., Hoen, M., and Baskin, D.G. (2003). Expression of receptors for insulin and leptin in the ventral tegmental area/substantia nigra (VTA/SN) of the rat. Brain Res. *964*, 107–115.

Floresco, S.B., West, A.R., Ash, B., Moore, H., and Grace, A.A. (2003). Afferent modulation of dopamine neuron firing differentially regulates tonic and phasic dopamine transmission. Nat. Neurosci. *6*, 968–973.

Ghosh, K.K., Burns, L.D., Cocker, E.D., Nimmerjahn, A., Ziv, Y., Gamal, A.E., and Schnitzer, M.J. (2011). Miniaturized integration of a fluorescence microscope. Nat. Methods *8*, 871–878.

Godfrey, N., and Borgland, S.L. (2019). Diversity in the lateral hypothalamic input to the ventral tegmental area. Neuropharmacology *154*, 4–12.

Gong, S., Doughty, M., Harbaugh, C.R., Cummins, A., Hatten, M.E., Heintz, N., and Gerfen, C.R. (2007). Targeting Cre recombinase to specific neuron populations with bacterial artificial chromosome constructs. J. Neurosci. *27*, 9817–9823.

Grace, A.A., and Bunney, B.S. (1984). The control of firing pattern in nigral dopamine neurons: single spike firing. J. Neurosci. *4*, 2866–2876.

Han, W., Tellez, L.A., Perkins, M.H., Perez, I.O., Qu, T., Ferreira, J., Ferreira, T.L., Quinn, D., Liu, Z.-W., Gao, X.-B., et al. (2018). A Neural Circuit for Gut-Induced Reward. Cell *175*, 665–678.e23.

Izumida, Y., Yahagi, N., Takeuchi, Y., Nishi, M., Shikama, A., Takarada, A., Masuda, Y., Kubota, M., Matsuzaka, T., Nakagawa, Y., et al. (2013). Glycogen shortage during fasting triggers liver-brain-adipose neurocircuitry to facilitate fat utilization. Nat. Commun. *4*, 2316.

Jennings, J.H., Ung, R.L., Resendez, S.L., Stamatakis, A.M., Taylor, J.G., Huang, J., Veleta, K., Kantak, P.A., Aita, M., Shilling-Scrivo, K., et al. (2015). Visualizing hypothalamic network dynamics for appetitive and consummatory behaviors. Cell *160*, 516–527.

Jin, X., and Costa, R.M. (2010). Start/stop signals emerge in nigrostriatal circuits during sequence learning. Nature *466*, 457–462.

Kaelberer, M.M., Buchanan, K.L., Klein, M.E., Barth, B.B., Montoya, M.M., Shen, X., and Bohórquez, D.V. (2018). A gut-brain neural circuit for nutrient sensory transduction. Science *361*, eaat5236.

Klaus, A., Martins, G.J., Paixao, V.B., Zhou, P., Paninski, L., and Costa, R.M. (2017). The Spatiotemporal Organization of the Striatum Encodes Action Space. Neuron *95*, 1171–1180.e7.

Klok, M.D., Jakobsdottir, S., and Drent, M.L. (2007). The role of leptin and ghrelin in the regulation of food intake and body weight in humans: a review. Obes. Rev. *8*, 21–34.

Lopes, G. (2015). Bonsai: An event-based framework for processing and controlling data streams. Frontiers in Neuroinformatics *9*, https://doi.org/10.3389/fninf.2015.00007.

Mason, M.R.J., Ehlert, E.M.E., Eggers, R., Pool, C.W., Hermening, S., Huseinovic, A., Timmermans, E., Blits, B., and Verhaagen, J. (2010). Comparison of AAV serotypes for gene delivery to dorsal root ganglion neurons. Mol. Ther. *18*, 715–724.

Naleid, A.M., Grace, M.K., Cummings, D.E., and Levine, A.S. (2005). Ghrelin induces feeding in the mesolimbic reward pathway between the ventral tegmental area and the nucleus accumbens. Peptides *26*, 2274–2279.

Oliveira-Maia, A.J., Roberts, C.D., Walker, Q.D., Luo, B., Kuhn, C., Simon, S.A., and Nicolelis, M.A.L. (2011). Intravascular food reward. PLoS ONE *6*, e24992.

Parker, J.G., Zweifel, L.S., Clark, J.J., Evans, S.B., Phillips, P.E.M., and Palmiter, R.D. (2010). Absence of NMDA receptors in dopamine neurons attenuates dopamine release but not conditioned approach during Pavlovian conditioning. Proc. Natl. Acad. Sci. USA *107*, 13491–13496.

Paxinos, G., and Franklin, K. (2008). The Mouse Brain in Stereotaxic Coordinates, 3rd (Elsevier Academic Press).

Pnevmatikakis, E.A., et al. (2016). Simultaneous Denoising, Deconvolution, and Demixing of Calcium Imaging Data. Neuron *89*, 285–299.

Qu, T., Han, W., Niu, J., Tong, J., and de Araujo, I.E. (2019). On the roles of the Duodenum and the Vagus nerve in learned nutrient preferences. Appetite *139*, 145–151.

Ramsey, A.J., Milenkovic, M., Oliveira, A.F., Escobedo-Lozoya, Y., Seshadri, S., Salahpour, A., Sawa, A., Yasuda, R., and Caron, M.G. (2011). Impaired NMDA receptor transmission alters striatal synapses and Dros. Inf. Serv.C1 protein in an age-dependent manner. Proc. Natl. Acad. Sci. USA *108*, 5795–5800.

Resendez, S.L., Jennings, J.H., Ung, R.L., Namboodiri, V.M.K., Zhou, Z.C., Otis, J.M., Nomura, H., McHenry, J.A., Kosyk, O., and Stuber, G.D. (2016). Visualization of cortical, subcortical and deep brain neural circuit dynamics during naturalistic mammalian behavior with head-mounted microscopes and chronically implanted lenses. Nat. Protoc. *11*, 566–597.

Sclafani, A. (2004). Oral and postoral determinants of food reward. Physiol. Behav. *81*, 773–779.

Sclafani, A., and Lucas, F. (1996). Abdominal vagotomy does not block carbohydrate-conditioned flavor preferences in rats. Physiol. Behav. *60*, 447–453.

Sclafani, A., Zukerman, S., and Ackroff, K. (2015). Postoral glucose sensing, not caloric content, determines sugar reward in C57BL/6J mice. Chem. Senses *40*, 245–258.

Steinbusch, L., Labouèbe, G., and Thorens, B. (2015). Brain glucose sensing in homeostatic and hedonic regulation. Trends Endocrinol. Metab. *26*, 455–466.

Sternson, S.M., Nicholas Betley, J., and Cao, Z.F.H. (2013). Neural circuits and motivational processes for hunger. Curr. Opin. Neurobiol. *23*, 353–360.

Su, Z., Alhadeff, A.L., and Betley, J.N. (2017). Nutritive, Post-ingestive Signals Are the Primary Regulators of AgRP Neuron Activity. Cell Rep. *21*, 2724–2736.

Tanahira, C., Higo, S., Watanabe, K., Tomioka, R., Ebihara, S., Kaneko, T., and Tamamaki, N. (2009). Parvalbumin neurons in the forebrain as revealed by parvalbumin-Cre transgenic mice. Neurosci. Res. *63*, 213–223.

Tellez, L.A., Han, W., Zhang, X., Ferreira, T.L., Perez, I.O., Shammah-Lagnado, S.J., van den Pol, A.N., and de Araujo, I.E. (2016). Separate circuitries encode the hedonic and nutritional values of sugar. Nat. Neurosci. *19*, 465–470.

Ueno, A., Lazaro, R., Wang, P.Y., Higashiyama, R., Machida, K., and Tsukamoto, H. (2012). Mouse intragastric infusion (iG) model. Nat. Protoc. *7*, 771–781.

Wise, R.A. (2006). Role of brain dopamine in food reward and reinforcement. Philos. Trans. R. Soc. Lond. B Biol. Sci. *361*, 1149–1158.

Zafra, M.A., Molina, F., and Puerto, A. (2007). Learned flavor preferences induced by intragastric administration of rewarding nutrients: role of capsaicin-sensitive vagal afferent fibers. Am. J. Physiol. Regul. Integr. Comp. Physiol. *293*, R635–R641.

Zhang, Y., Hoon, M.A., Chandrashekar, J., Mueller, K.L., Cook, B., Wu, D., Zuker, C.S., and Ryba, N.J.P. (2003). Coding of sweet, bitter, and umami tastes: different receptor cells sharing similar signaling pathways. Cell *112*, 293–301.

Zhang, L., Han, W., Lin, C., Li, F., and de Araujo, I.E. (2018). Sugar metabolism regulates flavor preferences and portal glucose sensing. Front. Integr. Neurosci. *12*, 57.

Zhou, P., Resendez, S.L., Rodriguez-Romaguera, J., Jimenez, J.C., Neufeld, S.Q., Stuber, G.D., Hen, R., Kheirbek, M.A., Sabatini, B.L., Kass, R.E., and Paninski, L. (2016). Efficient and accurate extraction of in vivo calcium signals from microendoscopic video data. Elife, *7*, e28728.

Zukerman, S., Ackroff, K., and Sclafani, A. (2011). Rapid post-oral stimulation of intake and flavor conditioning by glucose and fat in the mouse. Am. J. Physiol. Regul. Integr. Comp. Physiol. *301*, R1635–R1647.

Zweifel, L.S., Argilli, E., Bonci, A., and Palmiter, R.D. (2008). Role of NMDA receptors in dopamine neurons for plasticity and addictive behaviors. Neuron *59*, 486–496.

Zweifel, L.S., Parker, J.G., Lobb, C.J., Rainwater, A., Wall, V.Z., Fadok, J.P., Darvas, M., Kim, M.J., Mizumori, S.J.Y., Paladini, C.A., et al. (2009). Disruption of NMDAR-dependent burst firing by dopamine neurons provides selective assessment of phasic dopamine-dependent behavior. Proc. Natl. Acad. Sci. USA *106*, 7281–7288.

STAR★METHODS

KEY RESOURCES TABLE

REAGENT or RESOURCE	SOURCE	IDENTIFIER
Antibodies		
Anti-Tyrosine Hydroxylase antibody	Abcam	RRID: AB_112
Anti-Rabbit IgG H&L (Alexa Fluor® 555)	Abcam	RRID: AB_150078
Chicken polyclonal GFP antibody	Abcam	RRID: AB_13970
Anti-Chicken IgY H&L (Alexa Fluor® 488)	Abcam	RRID: AB_150173
Bacterial and Virus Strains		
AAV5.CAG.Flex.GCaMP6f.WPRE.SV40	UPENN	AV-5-PV2816
pAAV-CAG-GFP (AAV Retrograde)	Addgene	37825-AAVrg
AAV9.CAG.hChR2(H134R)-mCherry.WPRE.SV40	Addgene	100054-AAV9
pAAV-hSyn-hChR2(H134R)-EYFP (AAV1)	Addgene	26973-AAV1
pAAV-Ef1a-EYFP.hGH	Addgene	27056-AAV1
Chemicals, Peptides, and Recombinant Proteins		
Sucrose	Sigma-Aldrich	Cat# 84099
Sucralose	Sigma-Aldrich	Cat# 69293
Experimental Models: Organisms/Strains		
Mouse: B6;129-*Trpm5*^{tm1Csz}/J (Trpm5)	Jackson Laboratories	013068
Mouse: B6.Cg-*7630403G23Rik*$^{Tg(Th-cre)1Tmd}$/J (Th-Cre)	Gong et al., 2007; GENSAT Project MMRRC	RRID: MMRRC_017262-UCD
Mouse: B6.129S4-*Grin1*^{tm2Stl}/J (NR1Flox)	Jackson Laboratories; Zweifel et al., 2008	005246
Mouse: Slc6a3$^{tm1(cre)Xz}$/J (DAT-Cre)	Jackson Laboratories	020080
Software and Algorithms		
CNMF-e	Klaus et al., 2017; Pnevmatikakis, 2016	N/A
Bonsai-Open Ephys	Lopes, 2015	https://open-ephys.org/bonsai

LEAD CONTACT AND MATERIALS AVAILABILITY

Further information and requests for resources and reagents may be directed to and will be fulfilled by Lead Contact, Dr Rui Costa, rc3031@columbia.edu. This study did not generate new unique reagents.

EXPERIMENTAL MODEL AND SUBJECT DETAILS

All animal procedures were approved by the Champalimaud Foundation and Portuguese *Direção Geral de Veterinária*, and performed in accordance with the European Union Directive for Protection of Vertebrates Used for Experimental and other Scientific Ends (86/609/CEE and Law No. 0421/000/000/2014). Male C57BL/6J mice, purchased from Charles Rivers Laboratories, were tested between 3 and 4 months old. In some experiments, Transient Receptor Potential cation channel subfamily M member 5 (TRPM5) knock-out mice (Trpm5 KO mice) were used as one of the approaches to isolate postingestive feedback. In these mice, sweet taste transduction signaling is absent, resulting in abolished sweet taste palatability (Zhang et al., 2003). Male Trpm5 KO mice and WT littermates were bred from mice purchased from The Jackson Laboratory Stock 013068 (B6;129-Trpm5tm1Csz/J) and tested between 3 and 4 months old.

Cell-type specific deletion of the N-Methyl-D-aspartate receptor 1 subunit (NMDAR1) was achieved by breeding the *Th*-Cre mouse line (BAC Cre Line ER69), expressing Cre-recombinase in tyrosine hydroxylase gene (*Th*) mostly in VTA, and mice floxed for *Grin1* gene (encoding the NR1 subunit of NMDARs). Two-step breeding steps were performed: *Th*-Cre × *Grin1*$^{flox/flox}$ followed by *Th*-Cre:*Grin1*$^{flox/+}$ × *Grin1*$^{flox/flox}$ or *Grin1*$^{flox/+}$. Littermates with either *Th*-Cre or *Grin1*$^{flox/flox}$ genotypes were used as controls. NR1KO mice in dopamine neurons (referred as Th-CreNR1KO) and littermate control mice were tested between 2 and 4 months old. For calcium imaging studies, the male DAT-IRES:Cre (Dopamine Transporter-Internal Ribosome Entry Site-linked Cre recombinase gene) mouse line from Jackson Labs Stock 006660 (The Jackson Laboratory; B6.SJL-Slc6a3tm1.1(Cre)Bkmn/J) was used.

These mice have Cre recombinase expression directed to dopaminergic neurons, without disrupting endogenous dopamine transporter expression. Genotype was confirmed by polymerase chain reaction (PCR) amplification. Sample size is detailed in the Results and/or figure legends.

METHOD DETAILS

Reagents

Sucrose 0.6 M and sucralose (1,6 – Dichloro - 1,6 - dideoxy-β-D-fructofuranosyl −4 – chloro – 4 – deoxy -α-D-galactopyranoside) 0.5 mM solutions (Sigma-Aldrich) were prepared daily at room temperature in tap water. The chosen concentrations were based on previous work (Beeler et al., 2012) that showed the minimum concentration of either reinforcer necessary to ensure maximum licking.

Surgical procedures

Gastric catheter implantation

Animals were anesthetized using a mix of oxygen (1-1.5 l/min) and 1%–3% isoflurane, and the procedure conducted as described previously (Ueno et al., 2012), in aseptic conditions. Briefly, the hair on the mid abdomen and dorsal neck areas was clipped, the mouse was placed on a surgical table covered with a heating pad set at 37°C, and a midline incision was made into the abdomen. The stomach was exteriorized and a purse string suture (non-absorbable sutures, Vicryl, Johnson and Johnson), was placed in the proximal part of the stomach, into which the tip of a polyethylene tube (Instech Solomon) was inserted. The purse string was tightened around the tube, the other extremity of which was then tunneled subcutaneously to the dorsum and exteriorized through a small incision between the shoulder plates. Incisions were sutured (absorbable sutures, Vycril, Johnson and Johnson) and disinfected, and the externalized extremity of the catheter was closed using a rubber stopper (Instech Solomon). After surgery the animal was placed in a clean home cage, and left on a heating pad until fully recovered. Postoperative analgesia was administered as needed.

Selective Hepatic Vagotomy

General surgical procedures were performed as described above and hepatic branch vagotomy as described previously (Izumida et al., 2013). Briefly, a midline abdominal incision was made, the stomach pulled down and the ligaments attaching the liver to the stomach cut. The esophageal-hepatic attachments were exteriorized carefully and the hepatic branch of the vagus nerve was selectively transected. Sham vagotomy consisted of the same surgical procedure except for transection of the vagus nerve. At the end of the experiments, hepatic vagotomy was confirmed post-mortem by epididymal fat pad weight (Vagotomized: 1.95 ± 0.1% of total body weight, n = 12; Sham: 1.64 ± 0.03% of total body weight, n = 11; p = 0.007, unpaired t test), as has been described previously (Izumida et al., 2013).

Viral Injections, GRIN lens implantation and baseplate fixation

In preparation for calcium imaging experiments in DAT-IRES:Cre mice (Resendez et al., 2016), general surgical procedures were performed as described above. The mouse head was stabilized in the stereotaxic apparatus (Koft), a skin incision was performed to expose the skull, connective and muscle tissue was carefully removed and the skull surface was leveled at less than 0.05mm by comparing the height of bregma and lambda, and also in medial-lateral directions. Unilateral viral injections were performed using glass pipettes with 3μl GCaMP6f viral stock solution (AAV5.CAG.Flex.GCaMP6f.WPRE.SV40 - UPENN), to target the VTA (AP: −2.98 and DL: ± 0.4mm from bregma; DV: −4.5mm from brain surface;Paxinos and Franklin, 2008). 1 μL viral solution was injected into the VTA (4.6 nL every 5 s) using nanoject II (Drummond Scientific), with the pipette retracted only twenty minutes after the injection was completed. After 2 to 4 weeks of GCaMP6f injection into the VTA, a 2-3mm craniotomy was made in the viral injection coordinates (AP: −2.98 and DL: ± 0.4mmm from bregma) and a blunted needle (Infusion Technologies) was lowered 1.5-2.0mm above the VTA, to prepare for lens implantation and minimize associated tissue damage. A gradient refractive index lens (GRIN lens, diameter: 0.5mm, length: 8.2mm; Inscopix) was then implanted in the VTA at −4.5 to −4.7mm from brain surface. The GRIN lens was fixed using superglue and black dental cement (Lang Dental Mfg.), anchored to three screws implanted into the skull, with a layer of lens paper and adhesive tape applied to the top of the head cap to prevent lens damage. Two weeks after GRIN lens implantation, mice were secured in the stereotaxic apparatus under isoflurane anesthesia, the lens was exposed and a baseplate attached to the miniature microscope (nVistaHD, Inscopix) was positioned above it. The focal plane was adjusted for observation of neuronal structures and black cement used to permanently secure the baseplate to the head cap prior to removing the microscope and attaching a baseplate cover (Inscopix) to the baseplate. After baseplate fixation, a gastric catheter was implanted and, when applicable, hepatic vagus nerve lesions were performed, as described previously.

Surgery to implant multi-electrode arrays in the mouse brain

Multi-electrode arrays were implanted to record neural activity in freely moving mice, as described previously (Costa et al., 2006). Micro-electrode arrays consisted of two rows, separated by 200 μm, of eight polyamide-coated tungsten microwires with 35 μm diameter platinum plated tips, and inter-electrode spacing within each row of 150 μm (CD Neural Technologies, NC). To target the VTA, the center of the array was placed at 3.05 mm posterior and 0.75 mm left to Bregma, with electrodes lowered to 4–4.25 mm below the brain surface. Arrays were then fixed in place by dental acrylic. Animals were allowed to recover for at least 2 weeks before experiments started. Placement of electrodes was verified post-mortem by immunofluorescence staining for Th in 40 μm thick brain slices.

Behavioral Training

Behavior training took place in operant chambers (21.6 cm L x 17.8 cm W x 12.7 cm H), housed within sound attenuating chambers (Med-Associates). Each chamber was equipped with two retractable levers, one on either side of the food magazine, with a house light (3 W, 24V) mounted on the opposite side of the chamber. Each session began with the illumination of the house light and insertion of one or both levers, and ended with retraction of the lever(s) and offset of the house light. Water or sucrose or sucralose solutions were delivered into a metal cup in the magazine, and/or infused directly into the stomach through an intragastric catheter, using a syringe pump. The general behavioral protocol for instrumental conditioning was very similar across groups (Dias-Ferreira et al., 2009). Mice were trained in consecutive days, at approximately the same time of day. Briefly, training started with a 30 minute session where the reinforcer was delivered into the metal cup on a random time schedule, on average every 60 s. In the following days, delivery of the reinforcer was contingent on pressing a lever, initially on a continuous reinforcement (CRF) schedule, in which animals obtained a reinforcer after each lever press, progressing to a random ratio (RR) schedule, as described below. Sessions ended after 60 minutes or when mice received 30 reinforcers, whichever happened first. At the beginning of the protocol, mice were under a food and water deprivation schedule, receiving 1.5-2g of food and up to 30 minutes of free access of water after each training session, in order to maintain at least 85% of baseline body weight. Training progressed with interruption of water deprivation. During training, timestamps of lever presses, reinforcer delivery, licks and head entries were recorded with 10-ms resolution, allowing for a detailed analysis of the behavior of each animal across each session.

One lever instrumental task

Mice were trained with a single lever on a CRF schedule, with lever pressing leading to water for oral consumption. After acquisition of lever pressing behavior, water was replaced by sucrose (0.6 M) in some animals and sucralose (0.5 mM) in others. After the 6^{th} CRF session water deprivation was discontinued and after the 9^{th} CRF session, mice were tested on RR schedules, receiving one reinforcer after an average of 2 (RR2) or 4 (RR4) lever presses. In mice with intragastric catheters, training was conducted as described above (CRF-RR2-RR4) but, instead of delivering sucrose or sucralose for oral consumption, the reinforcer was delivered directly into the stomach, with water deprivation and delivery of water for oral consumption gradually discontinued after consolidation of lever pressing.

Two lever instrumental task

The two-lever instrumental task was conducted in a group of previously untrained C57Bl6/J animals, with two intragastric catheters, and both left and right levers extended into the chamber for training on a CRF schedule. Initially, food and water deprived mice could press either lever to obtain water for oral consumption. After acquisition of lever pressing behavior, intragastric infusions were initiated contingent upon lever pressing and concomitantly to delivery of water for oral consumption, with one lever leading to sucrose delivery and the other lever leading to sucralose delivery. The association between lever side and type of intragastric reinforcer was counterbalanced. Across 10 days of training, water deprivation and delivery of water for oral consumption were gradually interrupted, such that in the last 3 days of the protocol mice were pressing levers solely to obtain the intragastric infusions.

Electrophysiological Recordings

In vitro *slice recordings*

Horizontal or coronal slices (200–220 μm) containing the ventral midbrain were prepared from 4 to 8 weeks old Th-CreNR1KO and control littermate mice. Slices were allowed to recover at 33 ± 1°C for at least 45 min in artificial cerebro-spinal fluid (aCSF) containing the following (in mM): 126 NaCl, 2.5 KCl, 1.2 NaH_2PO_4, 1.2 $MgCl_2$, 2.4 $CaCl_2$, 11 glucose and 21.4 $NaHCO_3$, saturated with 95% O_2 and 5% CO_2, with pH 7.4 and osmolarity 300 mOsm/kg. They were then transferred to a recording chamber superfused with aCSF containing 50 μM picrotoxin at 2–3 ml/min, with temperature maintained at 33 ± 1°C during recording. Pipette solutions used for whole-cell and cell-attached recordings contained the following (in mM): 120 Cs methanesulfonate, 5 TEA-Cl, 2.8 NaCl, 20 HEPES, 0.4 EGTA, 2.5 Mg-ATP and 0.25 Na_2-GTP, with pH 7.2 - 7.3, and osmolarity 280 mOsm/kg. Putative midbrain dopamine neurons were identified by their locations relative to nearby anatomical landmarks and their spontaneous pacemaker firing at 0.5–5 Hz, monitored with cell-attached current-clamp configuration. Hyperpolarization-activated I_h currents were recorded immediately after entering the whole-cell voltage-clamp mode, but were not used as a sole dopamine neuron identifier. Membrane potential was first held at –55 mV to record I_h and to adjust the stimulator to achieve stable excitatory postsynaptic currents (EPSCs), then switched to +40 mV for the rest of the recording, with EPSCs evoked at 0.1 Hz with 50-500 μsec single square pulse of 50-1000 μA. NMDAR-mediated EPSCs were isolated pharmacologically by subtracting averaged traces in the presence of 50 μM APV (2-amino-5-phosphonovaleric acid, an NMDA receptor antagonist) applied to the bath, from the averaged control traces before and after washing out APV. A 700B amplifier (Molecular Devices) was used to record the data, which were filtered at 1–2 kHz, digitized at 2–5 kHz, and collected using pCLAMP software (Molecular Devices).

In vivo *extracellular recordings in mice*

Single-unit activity was recorded using the MAP system (Plexon Inc, TX), with time-stamps of behavioral events fed into the MAP system from the operant box (Med Associates Inc, VT), as decribed previously (Costa et al., 2006). Recordings were obtained while mice performed a classical conditioning task, with a 10 s house light and a 10 s, 3 kHz, 75 dB tone used as CS+ and CS-, respectively. At the onset of each CS+, a drop of sucrose solution was delivered to the tip of a feeding tube. CS- was not paired with any reward. CS+ and CS- were generated independently on a random-interval 120 s schedule (RI120). Animals were trained once daily until 30 rewards were received. Neural activity was first sorted online using Sortclient (Plexon Inc, TX), and then re-sorted based on wave-

forms using Offline Sorter (Plexon Inc, TX). Time stamps of sorted units and behavioral events were analyzed and plotted using Neuroexplorer (Nex Technologies, MA). Single units of DA neurons were identified by the following 3 criteria: AP waveform (distance from the first peak or to the last peak) longer than 1 ms, basal firing rate less than 10 Hz, and sensitivity to a type 2 dopamine receptor agonist quinpirole (200μg/kg, i.p., ~80% inhibition in 5 minutes). The onset of a burst was defined by an inter-spike interval (ISI) < 80ms, whereas the termination of a burst was defined by a interspike-interval (ISI) > 160 ms (Grace and Bunney, 1984).

Calcium Imaging

DAT-IRES:Cre mice implanted with a GRIN lens in the VTA and with an intragastric catheter, as described above, were placed on a food deprivation schedule, receiving 1.5-2g of food after each training session, in order to allow for maintenance of body weight of at least 85% of baseline weight. For the non-food deprived protocol, animals had *ad libitum* access to food in their home cage. Before each imaging session, mice were anesthetized with isoflurane, the baseplate cover and the lens cover were removed, and the microscope was attached to the baseplate.

Image acquisition

Fluorescence images were acquired using the nVista HD acquisition software (Inscopix) after a 30-min acclimatization period to allow for full recovery from anesthesia. Images were acquired at 10 Hz, with LED power set at 20%–40%, and gain level 4. Acquisition features were initially adjusted for each mouse but then kept constant across different test sessions. Each session began with the illumination of the house light and animals were allowed to freely move in the MedPC box throughout the session. After 5-min, one of the two reinforcers was infused into the stomach (intragastric protocol), or delivered into the magazine cup (oral protocol) at a rate of approximately 7μl/sec during 90 s. The session ended 15 minutes after start of the injection. Behavior was recorded across the full session using a top mounted camera (GoPro, 30Hz or DFK31BF03 camera, at a rate of 30 frames per second) for offline analysis in Python using a custom-made software. Movement was calculated by subtracting frame-to-frame pixel changes in the video. For the oral protocols, timestamps of magazine entries and licks, detected respectively using an infrared beam and a contact lickometer, were recorded with 10-ms resolution. In each protocol, the experimental procedure was repeated in several consecutive days, with delivery of either sucrose (0.6M) or sucralose (0.5mM) in separate days, in pseudo-randomized order to avoid more than 2 consecutive days with the same reinforcer. Protocol duration was 6 to 10 days (3-5 sessions of each reinforcer). Once the imaging session was completed the baseplate cover was again attached to the baseplate.

Image processing

Images were processed using Mosaic analysis software (Inscopix) and MATLAB 2015A. Imaging data was first binned in the spatial domain. Movement was corrected and cropped to remove margin values filled by the registration. To extract calcium fluorescence responses associated to individual neurons, a constrained non-negative matrix factorization (CNMF) was used (Klaus et al., 2017; Zhou et al., 2016). CNMF has been proposed as a framework for simultaneously denoising, deconvolving and demixing calcium imaging data (Zhou et al., 2016). This framework identifies the cell locations and handles spatial overlaps between neurons. CNMF-E is one of its extensions specialized for processing microendoscopic data. It can reliably address large fluctuating background from multiple sources, allowing for accurate source extraction of cellular signals. It includes four steps: (1) initialize spatial and temporal components of single neurons without the direct estimation of the background; (2) estimate the background given the estimated neuronal spatiotemporal activity; (3) update the spatial and temporal components of all neurons while fixing the estimated background fluctuations; (4) iteratively repeat steps 2 and 3.

Receiver operating characteristic (ROC) analysis

To characterize the responses of VTA dopaminergic neurons, we used a method similar to that described previously (Cohen et al., 2012). We measured the temporal response profile of GCaMP6f trace from baseline (180 s before reinforcer delivery) in 10 s bins using a receiver operating characteristic (ROC) analysis. For each neuron we compared the histogram of GCaMP6f trace during baseline to the respective GCaMP6f trace during each bin by moving a criterion from zero to the maximum fluorescence value during baseline. To produce the ROC for each bin after baseline, we plotted the probability that the activity during that bin was greater than the criterion, against the probability that baseline activity was greater than the criterion. We then calculated the area under the ROC curve (auROC) at each time bin, using trapezoidal numerical integration, with values lower than 0.5 denoting that activity in that bin is lower than baseline, and values higher than 0.5 denoting that activity is higher than baseline activity.

VTA dopaminergic neurons classification

To classify neurons as positively or negatively modulated by reinforcer administrations, we used the method described by da Silva et al. (2018). Mean activity in 180 s of baseline was chosen as a threshold. Mean fluorescence changes (based on the ΔF traces) were calculated for consecutive 10 s bins across 300 s after reinforcer delivery. Neurons with at least three consecutive bins (30 s) that were 2.56 standard deviations above the baseline activity (99% confidence interval), or 1.96 standard deviations (95% confidence interval) below the mean baseline threshold of fluorescence, were categorized as positively or negatively modulated, respectively.

Cell pairing between sessions

Analysis of matched cells between different days/sessions was based on nearest neighbors cell maps, as described previously (Jennings et al., 2015). Briefly, using spatial maps from a reference image, cell maps from the sessions to be matched were registered to the reference image, with registered coordinates calculated by applying the registering transformation to original coordinates. To calculate nearest-neighbor distances between imaging sessions of the same animal, distances were measured in one of the sessions to the most proximate cell acquired from the session to match. Based on these metrics, pairs of neurons between 2 sessions

with a distance greater than 10 pixels were considered distinct neurons. Cell pairing between sessions is presented for the last recording sessions, comparing last intragastric sucrose and previous or following sucralose session.

Histology and immunohistochemistry

Once experiments were completed, animals were anesthetized with an intraperitoneal injection of ketamine-xylazine (100mg/kg and 5mg/kg respectively) and perfusion was performed with 1x phosphate buffered saline (PBS) and 4% paraformaldehyde (PFA). Brains were gently extracted and placed in 4% PFA overnight and then transferred to PBS at 4°C for further histological processing. Brains were then sectioned coronally in 50 μM slices using a vibratome (Leica VT1000S), and sections collected into a 24-well plate with PBS. After mounting on slides, images of sections were taken using a wide-field fluorescence microscope (Zeiss AxioImager), and the tip of the longest track was used to determine the anatomical location of the lens, which was then represented in the corresponding Allen Brain Atlas slice (Figure S5). In one DAT-IRES:Cre mouse, to image GCaMP6f virus infection and lens placement in the VTA simultaneously (Figure S2A), sections were placed in a confocal microscope (Zeiss LSM710) and Z stacks were acquired (675 μM x 675 μM x 4 μM: 40 μM interslice interval) in a tile that covered all of the VTA. All images were processed using Zen Blue 2.5 and ImageJ software. To characterize the expression pattern of Cre recombinase activity in *Th*-Cre mice, double immuno-staining for *Th* and GFP was performed in mice generated by crossing *Th*-Cre mice with floxed-stop-FRP-GFP reporter mice. Coronal brain slices were stained with rabbit polyclonal anti-Th (1:1500) and chicken polyclonal anti-GFP (1:1000) primary antibodies (Abchem), and then with Alexa350 conjugated anti-rabbit (1:500) and Alexa488 conjugated anti-chicken (1:500) secondary antibodies (Molecular Probes).

Liver viral injections and Left Nodose Ganglion histological processing

For hepatic injections, in animals anesthetized with isoflurane-oxygen, a midline incision was made, the stomach pulled down and the ligaments attaching the liver to the stomach sectioned. The esophageal-hepatic attachments were carefully exteriorized and the hepatic vasculature and enervation exposed. Using Nanojet-II (Drumond Scientific) a retrograde AAVrg-CAG-GFP viral vector (Addgene), loaded into a beveled needle, was injected at 4.6nl every 5 s into the hepatic hylus. Three separate 0.5μl injections, separated 0.5cm from each other, in a total of 1.5μl, were performed. Four weeks after viral injections (Mason et al., 2010), animals were anesthetized with isoflurane and perfused with 1x PBS and 4% PFA. Both right and left nodose ganglion were gently extracted and placed in 4% PFA overnight and then transferred to PBS at 4°C for further immunobiological processing. To characterize the expression pattern of GFP activity in the nodose ganglion, NeuroTrace 530/615 red fluorescent Nissl staining was performed. Each nodose ganglion was placed in a confocal microscope equipped with a Diode 405nm, Argon multi-line 458-488-514nm and DPSS 561nm lasers (Zeiss LSM710). Z stacks were acquired (708.49 μm × 708.49 μm × 3 μm; 3-μm interslice interval) in a tile that covered all of the ganglion. All images were processed using Zen Blue 2.5 (Zeiss) and ImageJ (NIH) software.

For left nodose ganglion injections, a small incision above the trachea was performed. The vagus nerve was carefully isolated from the left carotid artery and followed until the laryngeal branch, after which the left nodose ganglion (LNG) was visualized and exposed. The viral vector AAV1-Syn-ChR2(H134R)-eYFP was loaded into the NanojetII and injected into the vagus nerve, as close as possible to the left nodose ganglion, at a rate of 2.3nl every 5 s, in a total of 0.5 μl. Four weeks after viral injections (Mason et al., 2010), animals were anesthetized with isoflurane and perfused with 1x PBS and 4% PFA. The left nodose ganglion was gently extracted and placed in 4% PFA overnight and then transferred to PBS at 4°C for further immunobiological processing. Each ganglion was imaged in a confocal microscope and images were processed as described above.

Left Nodose Ganglion stimulation protocol

Left nodose ganglion (LNG) injections were performed in DAT-IRES:Cre mice, as described above. A Cre-dependent adeno-associated viral vector AAV9.CAG.hChR2-mCherry.WPRE.SV40 (Addgene) or AAV1.EF1a.eYFP.hGH (YFP control) was injected. After virus injection, a small LED was carefully placed below the left vagus nerve and nodose ganglion, very close to the site of injection of the virus (Figure S6). LEDs were fixed using superglue, and the LED tube was tunneled subcutaneously to the dorsum and exteriorized between the shoulder plates. Incisions were sutured and disinfected, and the exterior part of the LED was weld to a connector. Two days after viral injections, stereotaxic surgery was performed for viral injection, GRIN lens implantation and baseplate placement, to allow for calcium imaging of VTA dopaminergic neurons, as described above. At this time point, the LED connector was glued to the cement cap and the LED was tested. Four weeks after all the surgical procedures, these DAT-IRES:Cre mice, food-restricted to maintain at least 85% of the initial body weight, were anesthetized with isoflurane, for removal of the baseplate and lens covers, and to attach the microscope to the baseplate. Fluorescence images were acquired as described above. After calcium imaging during 5 minutes, LNG stimulation was performed at 20Hz during 90 s and repeated every 180 s. The session ended 20 minutes after stimulation started, with the baseplate cover returned to its place. The experimental procedure was repeated daily in several consecutive days.

QUANTIFICATION AND STATISTICAL ANALYSIS

Data is presented as mean ± standard error of mean (SEM) and statistical significance was considered for $p < 0.05$. Statistical analysis was conducted using GraphPad Prism 6 (GraphPad Software Inc., CA), MATLAB statistical toolbox (The MathWorks

Inc, MA) and SPSS (IBM Analytics, NY). One-way, two-way or three-way ANOVAs were used to investigate main effects, and Bonferroni-corrected post hoc comparisons performed whenever appropriate. Paired or unpaired t tests were used for planned comparisons. Details for statistical tests are presented in supplementary Table S1. Statistical methods were not used to pre-determine sample size.

DATA AND CODE AVAILABILITY

The published article includes all datasets generated or analyzed during this study. Detailed datasets and codes supporting the current study are available from the corresponding authors on request.

Neuron, Volume *106*

Supplemental Information

Postingestive Modulation of Food Seeking Depends on Vagus-Mediated Dopamine Neuron Activity

Ana B. Fernandes, Joaquim Alves da Silva, Joana Almeida, Guohong Cui, Charles R. Gerfen, Rui M. Costa, and Albino J. Oliveira-Maia

Supplemental Information

Postingestive modulation of food seeking depends on vagus-mediated dopamine neuron activity

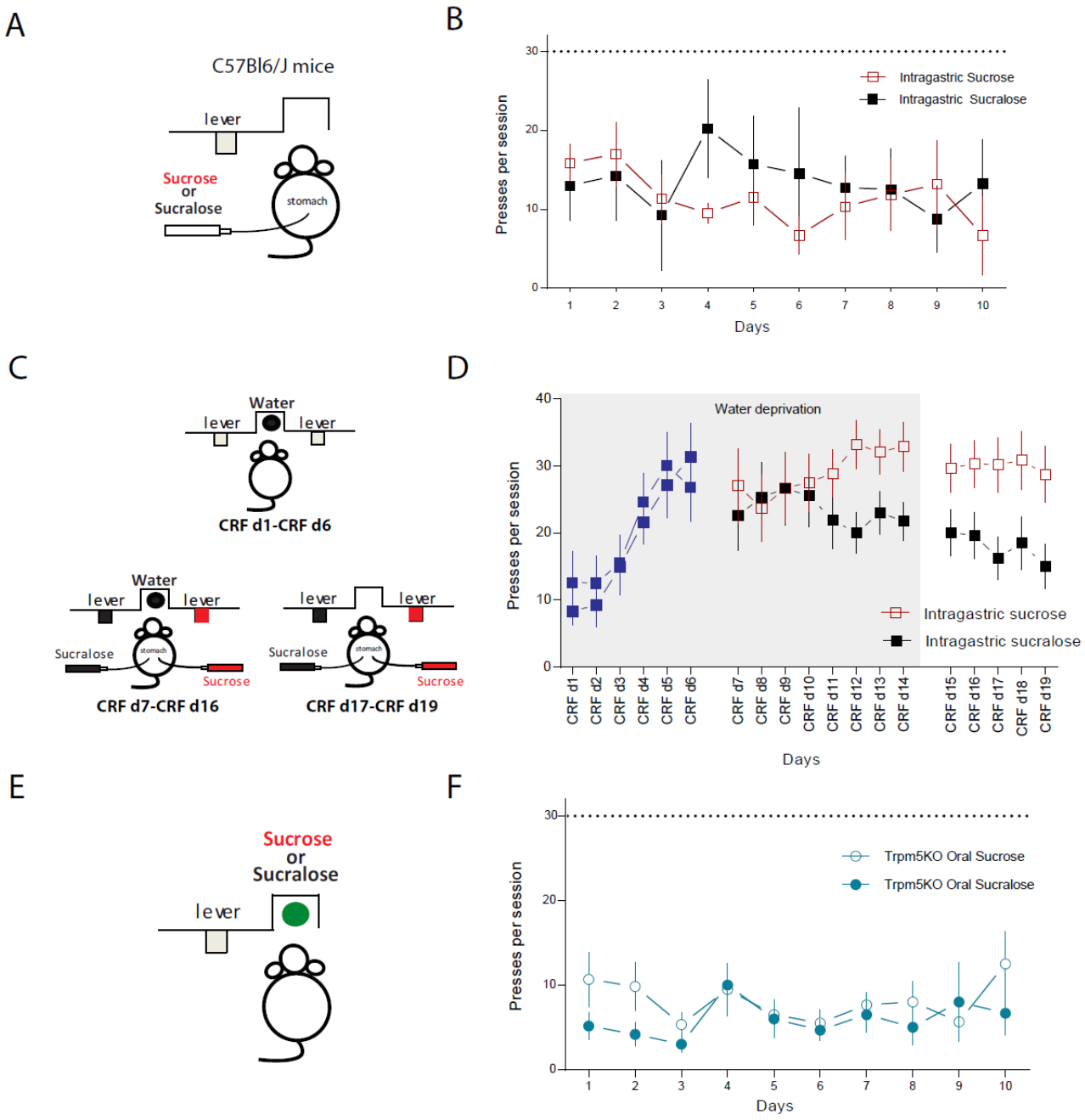

Figure S1: Postingestive modulation of food seeking (related to Figure 1). (A) Food deprived C57Bl6/J mice trained to press a lever to obtain intragastric infusion of either a sucrose solution, in one group of mice, or a sucralose solution, in another group. **(B)** Number of lever presses per session for intragastric sucrose infusion (n=6) compared to intragastric sucralose infusion (n=4; main effect for reinforcer: $F_{1,8}$=0.2, p=0.7; main effect for time: $F_{9,72}$=0.7, p=0.7; interaction: $F_{9,72}$=1.0, p=0.4; Two-way mixed ANOVA). **(C)** Simultaneous 2-lever choice task in C57Bl6/J mice with two intragastric catheters, enabling delivery of reinforcers directly into the stomach. Water and food deprived mice were trained to press 2 levers to obtain water for oral consumption (top panel). After acquisition of lever pressing, in addition to water for oral consumption, lever pressing also resulted in intragastric sucrose injection for one of the levers, and intragastric sucralose injection for the alternate lever. In the last 5 training days, water deprivation was discontinued and in the last 3 days, lever pressing resulted solely in intragastric infusion of the respective reinforcer (bottom panel). **(D)** Number of lever presses per session during the 2-lever choice task (n=14; main effect for reinforcer: $F_{1,26}$=2.8, p=0.1; main effect time: $F_{18,468}$=5.2,***, p<0.001; interaction: $F_{18,468}$=1.4, p=0.2; Two-way repeated measures ANOVA). Grey shading indicates water deprivation period. **(E)** Food deprived Trpm5

KO mice were trained daily for 10 days to press a lever to obtain an oral reinforcer (sucrose or sucralose). **(F)** Number of lever presses per session for Trpm5 KO mice when pressing the lever to obtain sucrose (n=6) or sucralose (n=6; main effect for reinforcer: $F_{1,10}$=1.2, p=0.3; main effect time: $F_{9,90}$=1.4, p=0.2; interaction: $F_{9,90}$=0.9, p=0.5; Two-way mixed ANOVA). Data are presented as mean ±SEM.

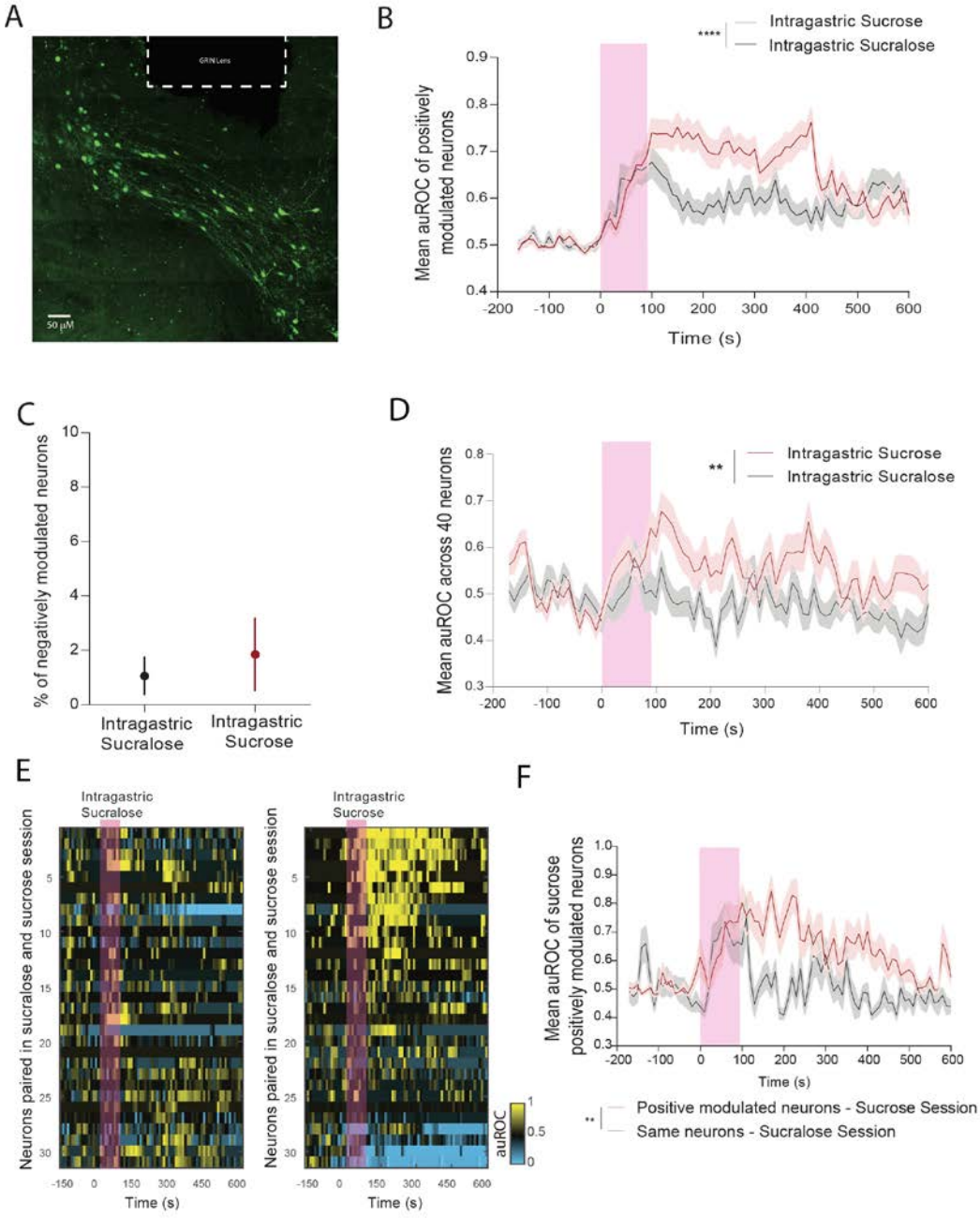

Figure S2: Activity of VTA dopaminergic neurons during intragastric infusion of reinforcers (related to Figure 2). (A) One example of a midbrain slice of DAT-IRES:Cre mouse showing GCaMP6f virus infection and the gradient lens (GRIN) placement in the VTA. **(B)** Activity of positively modulated VTA dopaminergic neurons in response to intragastric sucrose infusion (n=54 neurons) and in response to sucralose infusion (n=43 neurons; main effect for reinforcer: $F_{1,95}$=13.03, ****p=0.0005; main effect of time: $F_{77,7315}$=14.5, ***p<0.0001; interaction $F_{77,7315}$=4.4, ***p<0.0001; Two-way mixed ANOVA). **(C)** Comparison of the mean percentage of neurons per mouse that significantly decreased activity after infusion of either sucrose or sucralose (n=4; p=0.7; t=0.5; df=3; paired t-test). A neuron is considered negatively modulated if the fluorescence trace after the reinforcer delivery is below the 95% confidence interval of the baseline distribution (acquired during 180s prior to infusion) in 3 consecutive 10s bins (30s). **(D)** Mean activity of VTA dopaminergic neurons recorded both in the last sucrose and the following sucralose sessions (n=40; main effect of reinforcer: $F_{1,39}$=7.4, **p=0.01; main effect of time: $F_{77,3003}$=3.3, ****p<0.0001; interaction

$F_{77,3003}$=2.5, ****p<0.0001; Two-way repeated measures ANOVA). Shading represents SEM. **(E)** Tracking of 31 neurons recorded both in the last sucrose session (panel on the right) and the previous, rather than the following, sucralose session (panel on the left). Each line on both panels represents one neuron, with a color code for variation of neuronal activity relative to baseline (auROC, see methods) in consecutive 10s-long bins. **(F)** Among the neurons in E, 12 neurons were positively modulated in the intragastric sucrose session. Here we compare activity of these neurons in the sucrose and sucralose sessions (main effect for reinforcer: $F_{1,11}$=15.4, **p=0.002; main effect of time: $F_{77,847}$=6.4, ****p<0.0001; interaction reinforcer x time $F_{77,847}$=3.4, ****, p<0.0001; Two-way repeated measures ANOVA). Shading or error bars indicate SEM.

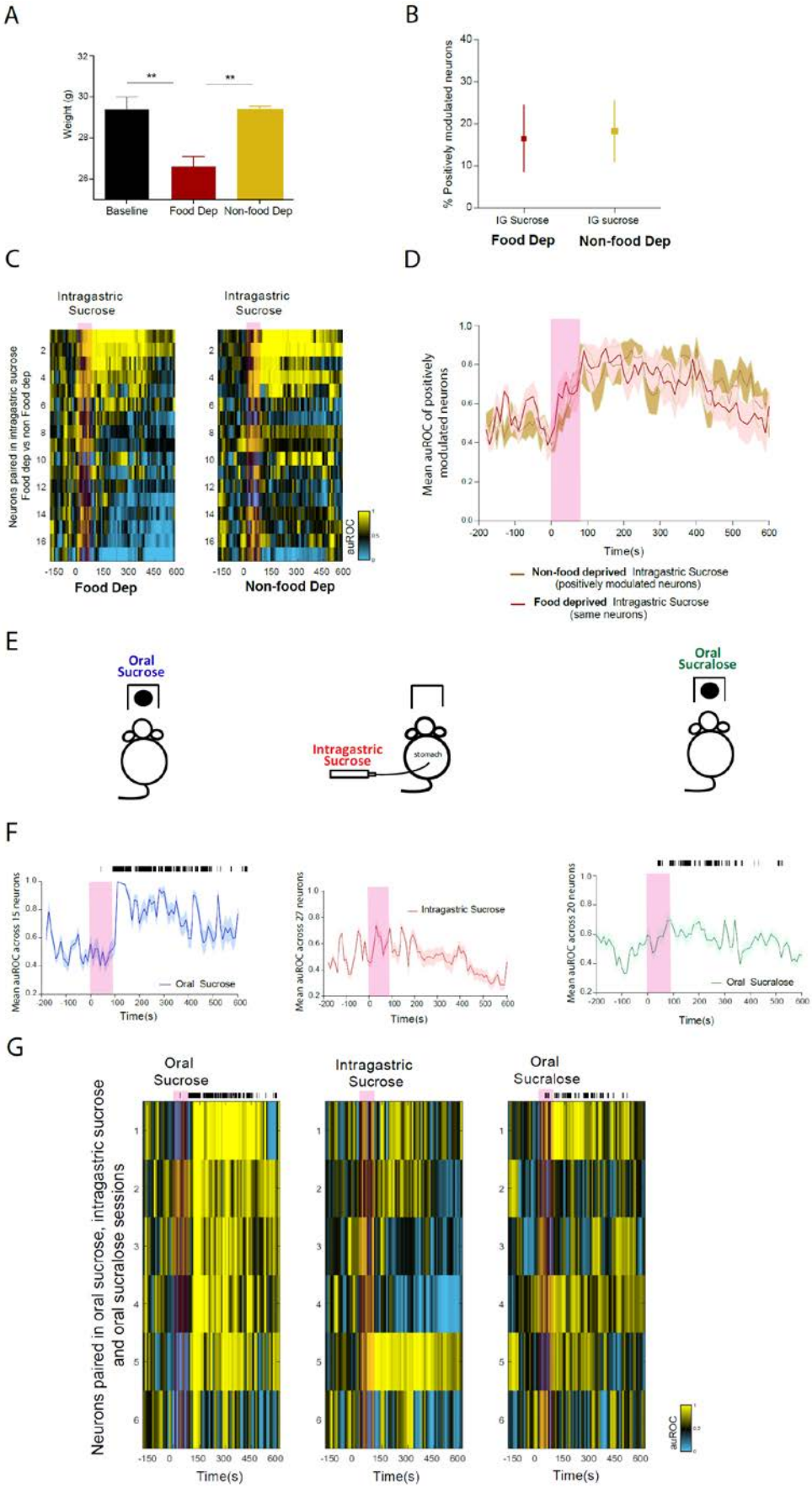
A
Weight (g)
Baseline
Food Dep
Non-food Dep
B
% Positively modulated neurons
IG Sucrose
IG sucrose
Food Dep
Non-food Dep
C
Intragastric Sucrose
Intragastric Sucrose
Neurons paired in intragastric sucrose Food dep vs non Food dep
auROC
Food Dep
Non-food Dep
D
Mean auROC of positively modulated neurons
Time(s)
Non-food deprived Intragastric Sucrose (positively modulated neurons)
Food deprived Intragastric Sucrose (same neurons)
E
Oral Sucrose
Intragastric Sucrose
stomach
Oral Sucralose
F
Mean auROC across 15 neurons
Oral Sucrose
Time(s)
Mean auROC across 27 neurons
Intragastric Sucrose
Time(s)
Mean auROC across 20 neurons
Oral Sucralose
Time(s)
G
Oral Sucrose
Intragastric Sucrose
Oral Sucralose
Neurons paired in oral sucrose, intragastric sucrose and oral sucralose sessions
Time(s)
Time(s)
Time(s)
auROC

Figure S3: Activity of VTA dopaminergic neurons under different stimulation protocols (related to Figure 2). In a new set of DAT-IRES:Cre mice infected with GCaMP6f virus and gradient lens (GRIN) placed in the VTA the effects of nutritional state were studied. **(A)** Weight of 3 DAT-IRES:Cre mice during 2 food deprived sessions and 2 non-food deprived sessions. Weight was collected at baseline (before training started), and before food-deprived and non-food deprived sessions. In the food deprivation schedule, mice received 1.5-2g of food after each session, in order to maintain at least 85% of baseline weight. During the non-food deprived protocol, mice had *ad libitum* access to food in their home cage (n=3, 2 sessions on Food Deprived protocol and 2 sessions on the non-Food-deprived schedule; One-way repeated measures ANOVA, $F_{1.4,2.8}$=18.4; *p=0.03, Bonferroni-corrected post-hoc tests, **p<0.01). Food and non-food deprivation schedules were randomized. **(B)** Analysis of mean percentage of neurons per session that significantly increased activity after sucrose administration when compared to 180 seconds of baseline activity across mice (n=3; p=0.2; paired t-test). A neuron is considered positively modulated if the fluorescence trace after the reinforcer delivery is above the 99% confidence interval of the baseline distribution in 3 consecutive 10s bins (30s). **(C)** Analysis of the activity of 17 neurons recorded both in the last sucrose session under food deprivation (left panel) and the following sucrose session conducted without food deprivation (right panel). Each line on both panels represents a single neuron, with a color code for variation of neuronal activity relative to baseline (auROC - see methods) in consecutive 10s-long bins. Red bar represents time of reinforcer injection. **(D)** Among the 17 neurons represented in C, 7 were positively modulated by intragastric sucrose in the food deprived session. Here, activity for these 7 neurons was compared between the food deprived and the non-food deprived sessions (n=7 neurons; main effect deprivation protocol: $F_{1,7}$=0.08, p=0.8; main effect time: $F_{170,1190}$=2.4, ****p<0.001; interaction: $F_{170,1190}$=0.9, p=0.8; Two-way repeated measures ANOVA). **(E)** In one DAT-IRES:Cre mouse infected with GCaMP6f virus and with a gradient lens (GRIN) placed in the VTA, the effect of reinforcer delivery route was studied, i.e. oral versus intragastric reinforcer delivery, under food deprivation. VTA dopaminergic neuron activity was measured during licking of sucrose in the magazine cup (left panel); intragastric delivery of sucrose (middle panel); licking of sucralose delivered in the magazine cup (right panel). In all cases, 0.6mL of the reinforcer was injected into the stomach or delivered in the magazine cup, across 90 seconds (pink bar in panels F and G). For oral consumption animals were allowed to lick freely until the end of the session. **(F)** Activity of VTA dopaminergic neurons during the 3 sessions (n=15 neurons for oral sucrose; n=27 neurons for intragastric sucrose; n=20 for oral sucralose). In the oral sessions black lines correspond to licks. Effect of reinforcer consumption/administration on VTA dopaminergic neuron activity was performed using the auROC analysis (see methods). Shading indicates SEM. **(G)** Activity of 6 neurons after oral sucrose delivery in the magazine cup, compared to the same neurons during intragastric sucrose infusion and the after oral sucralose delivery in the magazine cup. Neuronal activity is classified relative to baseline according to the auROC analysis. Shading or error bars indicate SEM.

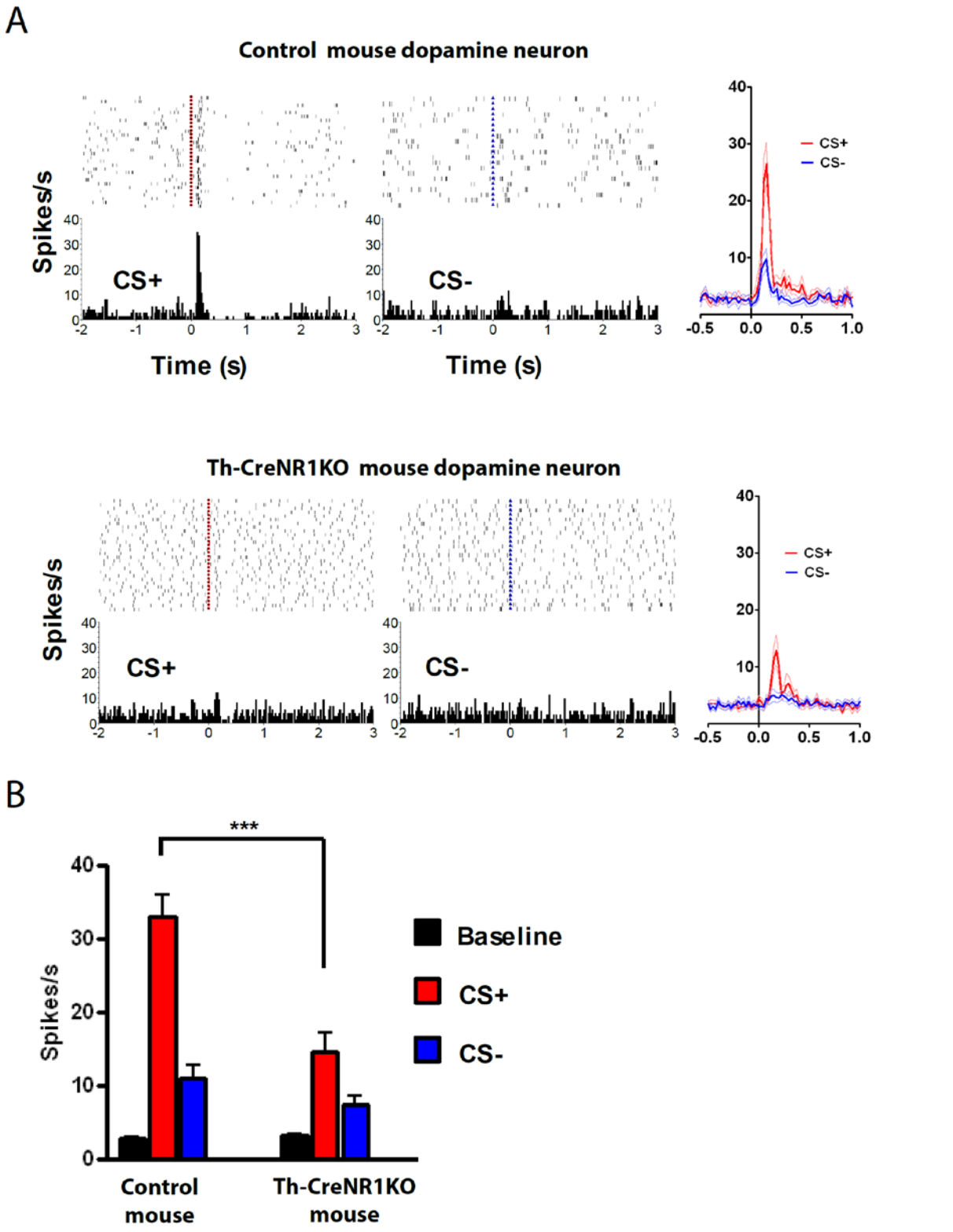

Figure S4: Th-CreNR1KO mice displayed attenuated cue-evoked burst firing in medial population (VTA) of dopamine neurons (related to Figure 3). (A) Examples of peri-event raster plot and histogram of a single dopamine neuron and **(B)** averaged population response of dopamine neurons aligned to the onset of a 10 second house light or tone (3 kHz, 75 dB), which were used as reward predictive (CS+) or non-reward predictive (CS-) cues, respectively. We recorded dopamine neuron activities from 8 Th-CreNR1KO mice and

5 control littermates during cue-evoked burst firing of dopamine neurons. At the onset of each CS+, a drop of sucrose solution was delivered to the tip of a feeding tube located in a recessed food magazine on the wall opposite to the house light and speaker. CS- was not paired with any reward. Deletion of NMDA receptors (NMDARs) in dopamine neurons caused a profound decrease in the magnitude of CS+ evoked responses in VTA dopamine neurons. The peak firing rate (measured from 75ms to 175ms after the onset of CS+) of VTA dopamine neurons was 33.0 ± 3.1 Hz (n = 13) in control animals and 14.5 ± 2.6 Hz (n = 24) in Th-CreNR1KO mice, respectively (***, $p<0.001$, t-test). Data is presented as mean±SEM.

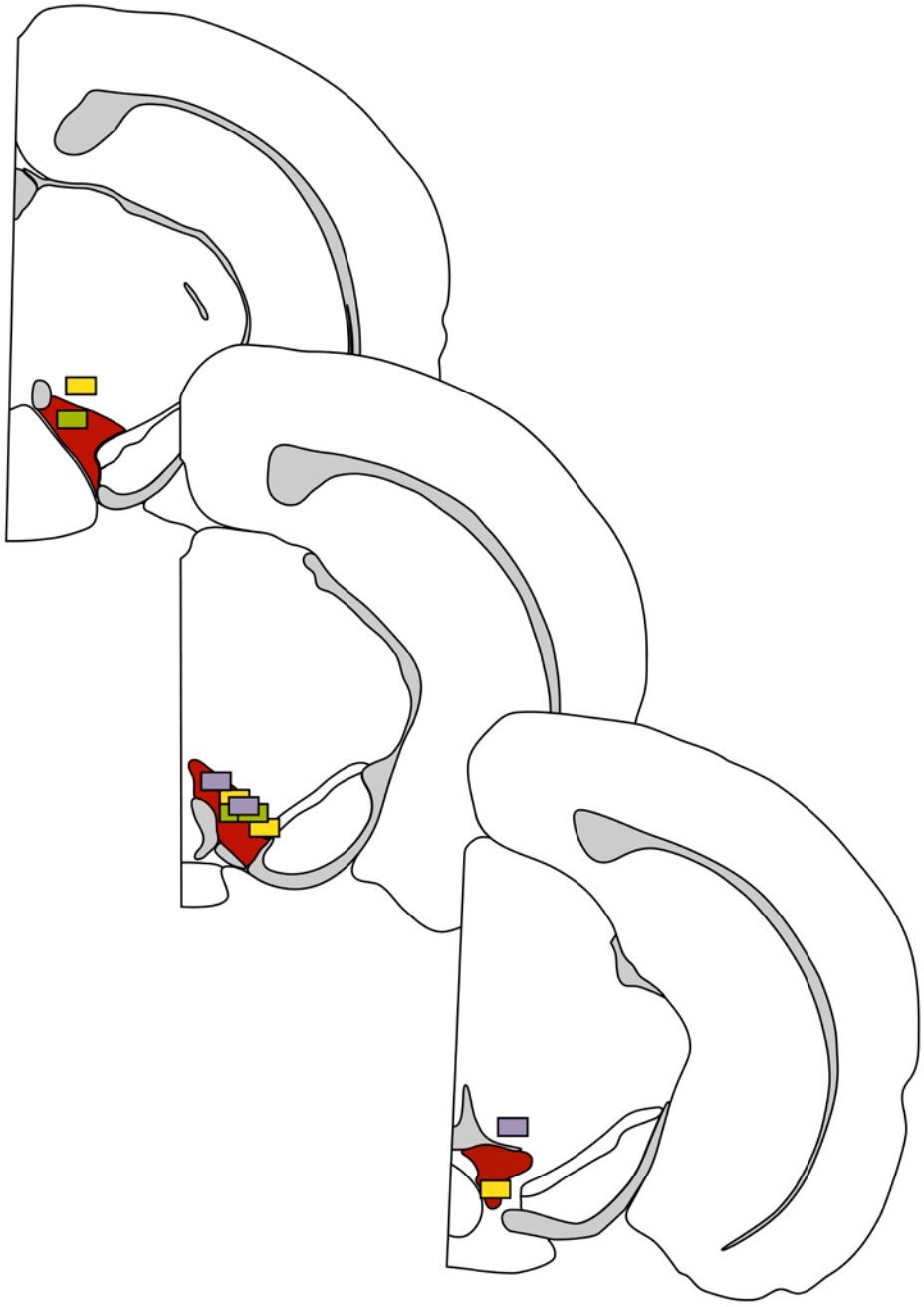

Figure S5: Anatomical position of the GRIN lens (related to Figures 2 and 4). The position of the tip of the GRIN lens is shown for each mouse where VTA dopaminergic activity was determined. Anatomical structures and their representation was obtained from the Allen mouse brain atlas using Application Programming Interface (API), and the VTA is represented in red. Yellow bars represent the positions for the initial group (Fig. 2), while green and purple bars respectively represent sham and denervated mice in the second imaging experiment (Fig. 4).

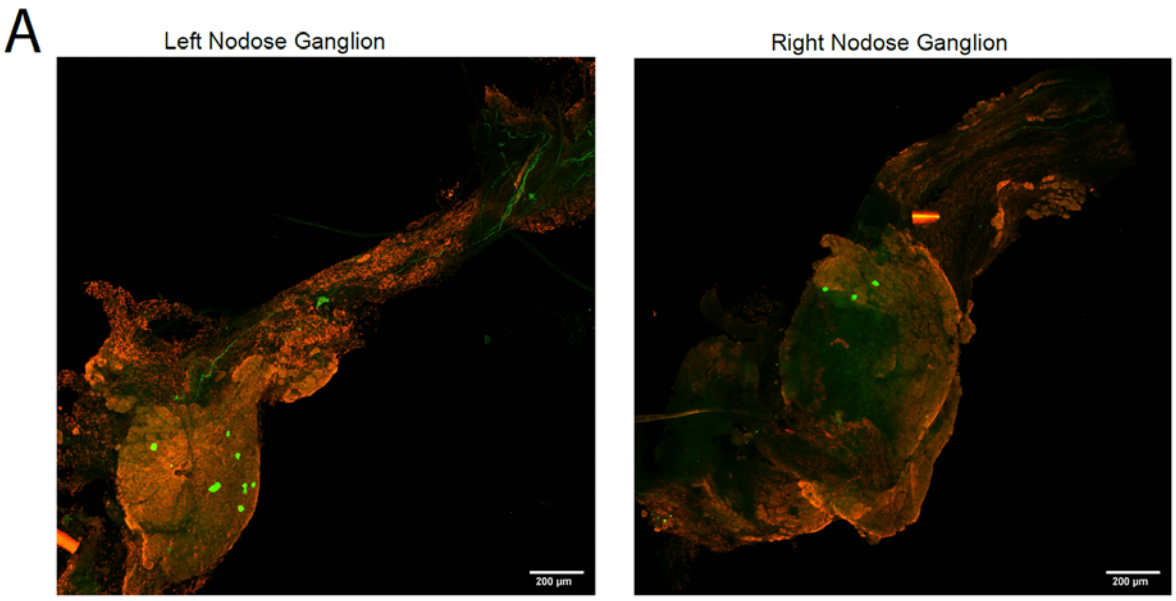
A
Left Nodose Ganglion
Right Nodose Ganglion
200 µm
200 µm

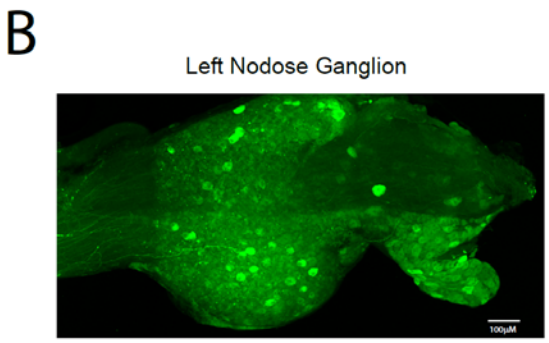
B
Left Nodose Ganglion
100µM

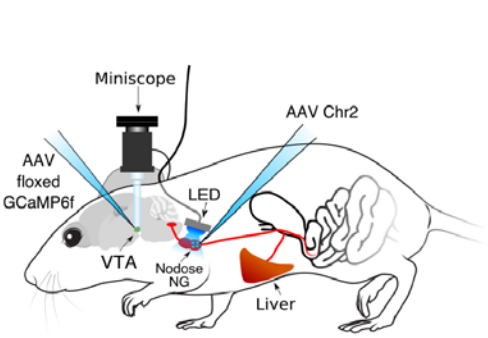
C
Miniscope
AAV Chr2
AAV
floxed
GCaMP6f
LED
VTA
Nodose
NG
Liver

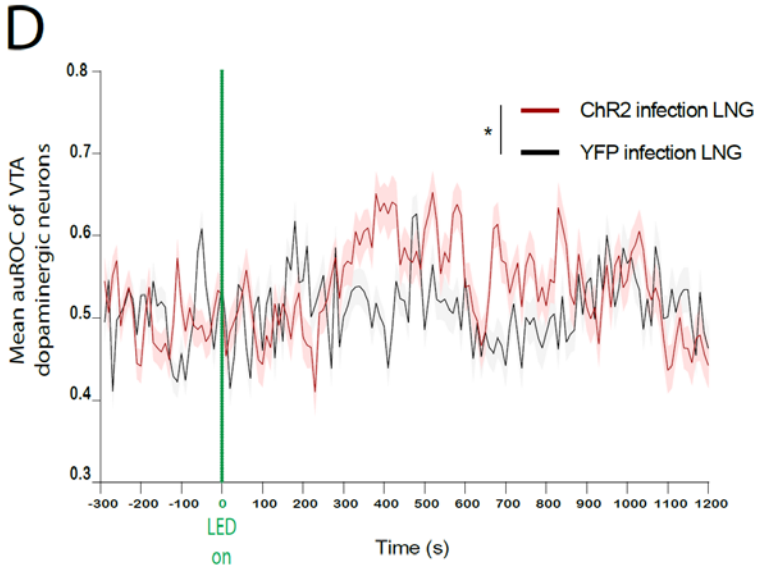
D
Mean auROC of VTA
dopaminergic neurons
0.8
0.7
0.6
0.5
0.4
0.3
*
ChR2 infection LNG
YFP infection LNG
-300 -200 -100 0 100 200 300 400 500 600 700 800 900 1000 1100 1200
LED
on
Time (s)

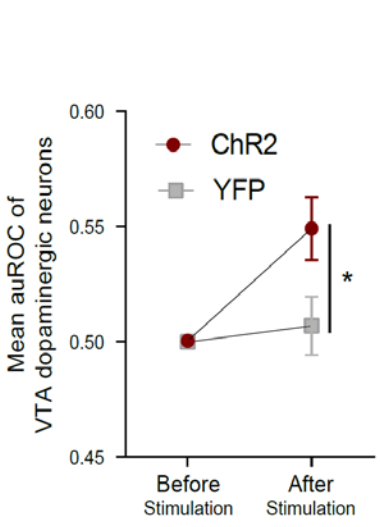
E
Mean auROC of
VTA dopaminergic neurons
0.60
0.55
0.50
0.45
ChR2
YFP
*
Before
Stimulation
After
Stimulation

Figure S6: Left Nodose Ganglion stimulation activates VTA dopamine neurons. (A) Left and right nodose ganglion immunostaining after retrograde AAV-GFP viral injection at the hepatic hylus, showing GFP-marked cell bodies and nerve fibers. **(B)** AAV1.hSyn.eGFP.ChR2 viral injection at the left nodose ganglion (LNG) showed immunostaining for GFP-marked cell bodies and nerve fibers. **(C)** Scheme of the method for optogenetic stimulation of the LNG using an LED, while activity of VTA dopamine neurons was recorded. Sessions were performed in the home cage. They began with illumination of the house light and animals were allowed to freely move throughout the session. After baseline calcium imaging during 5-min, the stimulation protocol was performed at 20Hz during 90 seconds and them repeated every 180 seconds. The session ended after 20 minutes of intermittent stimulation. **(D)** Time lapse of VTA dopaminergic neuron activity in DAT-IRES:Cre mice with LNG infections of either ChR2 (2 mice, 2 sessions, n=80 neurons) or YFP (2 mice, 2 sessions, n=84 neurons; main effect for reinforcer: $F_{1,162}$=5.1, *p=0.03; main effect time: $F_{90,14580}$=5.2, ****p<0.0001; interaction: $F_{90,14580}$=4.8, ****, p<0.0001; Two-way Mixed ANOVA). Effect of LNG stimulation on VTA dopaminergic neuron activity was performed using the auROC analysis (see methods). Shading indicates SEM. **(E)** Mean activity of VTA dopamine neurons 5 minutes before and 15 minutes after the start of the stimulation protocol according to auROC analysis (unpaired t-test, *p<0.05).

Table1: Statistical analysis (related to Figures 1, 2, 3 and 4)

Fig	Sample size (n)	Statistical test	Values
1B	Oral Sucrose: n=7; Oral Sucralose: n=7	Two-way mixed ANOVA; Multiple comparisons Bonferroni corrected;	*Main effect reinforcer $F_{(1,12)}$=5.989, p=0.04; ***Main effect time (training sessions): $F_{(9,108)}$=3.667, p=0.0005; Interaction $F_{(9,108)}$=1.494, p=0.16;
1D	Intragastric Sucrose: n=10; Intragastric Sucralose: n=12	Two-way mixed ANOVA; Multiple comparisons Bonferroni corrected;	****Main effect reinforcer $F_{(1,20)}$=87.13, p<0.0001; **** Main effect time (training sessions): $F_{(17,340)}$=11.45, p<0.0001; ****Interaction $F_{(17,340)}$=22.48, p<0.0001;
1F	Intragastric Sucrose/Intragastric Sucralose: n=13	Two-way repeated measures ANOVA	*Main effect reinforcer $F_{(1,12)}$=6.68, *p=0.02; Main effect time (training sessions): $F_{(12,144)}$=0.42, p=0.95; Interaction $F_{(12,144)}$=0.98, p=0.47;
1H	Control littermates Oral Sucrose: n=9; Control littermates Oral Sucralose: n=8; Trpm5KO Oral Sucrose: n=7; Trpm5 KO Oral Sucralose: n=8	Three-way mixed ANOVA (Genotype x Reinforcer x Time)	***Interaction time (training days) x Genotype: $F_{(12,324)}$=3.21, p=0.0002;
		Two-way mixed ANOVA (per genotype); Multiple comparisons Bonferroni corrected	**TRPM5 WT:** ***Main effect reinforcer $F_{(1,15)}$=15.43, p=0.001; ****Main effect time (training sessions): $F_{(12,180)}$=43.18, p<0.0001; ****Interaction: $F_{(12,180)}$=17.18, p<0.0001; **TRPM5KO:** ***Main effect reinforcer $F_{(1,12)}$=18.21, p=0.001; ****Main effect time (training sessions): $F_{(12,144)}$=17.74, p<0.0001; ****Interaction: $F_{(12,144)}$=15.12, p<0.0001;
2C	Intragastric Sucralose/Intragastric Sucrose: n=4	Paired t-test	p=0.2;
2D	Intragastric Sucralose/Intragastric Sucrose: n=4	Paired t-test	*p=0.03;
2F	Positively modulated neurons - Sucrose session/Sucralose session; n=18 neurons;	Two-way repeated measures ANOVA	****Main effect reinforcer: $F_{(1,17)}$=34.3, p<0.0001; ****Main effect time: $F_{(77,1309)}$=3.4, p<0.0001; ****Interaction $F_{(77,1309)}$=41.34, p<0.0001;
2G	Movement - Intragastric sucralose/Intragastric sucrose: n=3	Two-way repeated measures ANOVA	Main effect reinforcer: $F_{(1,2)}$=0.33, p=0.6; ****Main effect time: $F_{(80,160)}$=2.77, p<0.0001; Interaction $F_{(80,160)}$=1.24, p=0.13;
3B	Th^+expressing cells in VTA/SNc n=6 sections; Th^+expressing cells LC; n=4 sections;	Paired t-test	**p<0.01
3G	Control littermates, n=5 Th-CreNR1KO mice, n=14	Unpaired t-test	*p<0.05
3H	Control littermates, n=5 Th-CreNR1KO mice, n=14	Unpaired t-test	*p<0.05
3J	Control littermates intragastric Sucrose: n=6; Control littermates intragastric Sucralose: n=5; Th-CreNR1KO intragastric Sucrose: n=5; Th-CreNR1KO intragastric Sucralose: n=3;	Three-way mixed ANOVA (Genotype x Reinforcer x Time)	**Interaction: Time (training days) x Genotype: $F_{(17,255)}$=2.32, p=0.003;
		Two-way mixed ANOVA (per genotype);	**Control:** *Main effect reinforcer: $F_{(1,9)}$=7.84, p=0.02; ****Main effect time (training sessions): $F_{(17,153)}$=3.79, p<0.0001; ****Interaction: $F_{(17,153)}$=4.99, p<0.0001; **Th-CreNR1KO:** Main effect reinforcer: $F_{(1,6)}$=1.36, p=0.3; *Main effect time (training sessions): $F_{(17,102)}$=1.75, p=0.046; Interaction: $F_{(17,102)}$=17.65, p=0.3;
4A	Sham Surgery: n=3 Hepatic Vagotomy: n=3;	Unpaired t-test	p=0.4
4B	Sham surgery: Intragastric sucrose – n=249 neurons; Intragastric sucralose – n=221 neurons	Two-way mixed ANOVA	****Main effect reinforcer: $F_{(1,50544)}$=674.7, p<0.0001; ****Main effect time (training sessions): $F_{(107,50544)}$=8.59, p<0.0001; ****Interaction: $F_{(107,50544)}$=5.25, p<0.0001;
4C	Sham Surgery: n=3	Paired t-test	Sham surgery: *p=0.03;
4D	Hepatic Vagotomy: Intragastric sucrose – n=299 neurons; Intragastric sucralose - n=263 neurons	Two-way mixed ANOVA	Main effect reinforcer: $F_{(1,60480)}$=3.5, p=0.6; ****Main effect time (training sessions): $F_{(107,60480)}$=14.41, p<0.0001; ****Interaction: $F_{(107,60480)}$=2.6, p<0.0001;
4E	Hepatic Vagotomy: n=3	Paired t-test	Hepatic vagotomy: p=0.98
4H	Sham Surgery: n=46; Hepatic Vagotomy: n=50	Fisher test	**p=0.002
4J	Sham Surgery: n=8 Hepatic Vagotomy: n=9;	Two-way mixed ANOVA; Multiple comparisons Bonferroni corrected	Main effect intervention: $F_{(1,15)}$=3.79, p=0.07; ****Main effect time (training sessions): $F_{(17,255)}$=20.27, p<0.0001; ****Interaction: $F_{(17,255)}$=3.42, p<0.0001;